Three-dimensional ultrasound

Enabling volume measurements with a two-dimensional ultrasound probe

by

Stefan Johannes Fransen

in partial fulfilment of the requirements for the degree of

Master of Science

in Biomedical Engineering

at the Delft University of Technology,

to be defended publicly on Friday March 12, 2021 at 14:30.

Student number:	5016061	
Daily supervisor:	Dr. ir. T.L.A. van den Heuvel	Radboudumc
Thesis committee:	Dr. N. Bhattacharya	TU Delft
	Dr. K.W.A. van Dongen	TU Delft
	Dr. S. Iskander-Rizk	TU Delft

TU Delft Delft University of Technology

Radboudumc

Contents

ABSTRACT

This work investigates low-cost three-dimensional (3D) ultrasound reconstruction from a two-dimensional (2D) hand-held probe with motion tracking. The best available motion tracking is an optical tracking system, which is expensive and requires external tracking hardware. Here, a low-cost manoeuvrable motion tracker, an inertial measurement unit (IMU) sensor, has been tested by comparing it with an optical tracking system.

The motion of the probe has been divided into a rotation and translation movement. Comparing the IMU sensor rotation tracking with the optical tracking, while rotating 40 degrees, resulted in an average Pearson's correlation of 0.99 ± 0.0056. The average Pearson's correlation between the translation tracking of the IMU sensor and the optical tracking system, in a translation of 15 centimetres, was 0.13 ± 0.78. The rotation and translation tracking is used to reconstruct the ultrasound volume of a phantom. In a rocking motion reconstructed volume the horizontal distance between phantom features had a mean error of 45%, a vertical distance was reconstructed with a mean error of 0.25%. In a translation motion reconstructed volume these errors were 29% and 1.4% for respectively horizontal feature distance and vertical feature distance.

This study demonstrates that an IMU sensor can be used to track the motion of the probe. The rotation tracking of the IMU sensor is comparable with the rotation tracking of an optical tracking system. The translation tracking of the IMU sensor is on average not comparable with an optical tracking system, however some translations have been tracked with a high correlation. A reason to explain the low average correlation of the translation tracking of the IMU sensor is the method of gravity vector correction in the accelerometer data. Future research should focus on the clinical evaluation of the rotation tracking and the development of an accurate translation tracking method by studying the initial gravity vector or looking at different translation tracking methods.

NOMENCLATURE

2D	two-dimensional
3D	three-dimensional
B-scan	two-dimensional ultrasound image
IMU	inertial measurement unit

INTRODUCTION

3D ultrasound has been a well-studied topic in the literature over the past decades and has proven useful in clinical practice (Mozaffari & Lee, 2017a). In comparison with conventional 2D ultrasound images, a 3D ultrasound volume enables quantitative volume measurements of complex structures and cross-sectional imaging (Sofka et al., 2014). The advantages of 3D ultrasound imaging can potentially also be useful in automated ultrasound diagnostics.

This research is part of the BabyChecker project that aims to introduce prenatal screening in resource limited settings (van den Heuvel, 2019). The BabyChecker combines an ultrasound device with artificial intelligence to automatically detect prenatal risk factors. It makes use of the MicrUs Pro C60s (Telemed, Lithuania), which is a low-cost hand-held ultrasound device with integrated sensor that can be connected with an Android based smartphone. All automated analyses are currently performed on 2D ultrasound images. The initial goal of this study was to use the integrated sensor of the probe to create a 3D volume from these sweeps, to potentially enable volumetric measurements. However, the integrated sensor only contained an accelerometer, which on its own can't provide enough information for motion tracking, because a gyroscope is required to track the rotations. Instead, in this study the IMU sensor of a smartphone has been used, which has both an accelerometer and a gyroscope.

To acquire a 3D ultrasound volume from 2D ultrasound images, three steps can be defined: step one: 'motion tracking', 2D ultrasound image acquisition and simultaneously motion tracking, consisting of rotations and translation motion, of the probe; step two: 'transformation matrix calculation', calculate the transformation matrixes from the motion tracking data; and step three: 'volume reconstruction', reconstruction of the 3D ultrasound volume using the transformation matrixes to translate the pixels of the 2D ultrasound images into the voxels of a 3D volume grid. The methods for motion tracking can be divided into six categories, an overview of these methods and calibration techniques was made at the start of this project in a literature review, see appendix 1. In this paper the motion tracking of an IMU sensor is compared with the motion tracking of an optical system. An optical system is very accurate, but is expensive and requires external tracking hardware (Treece et al., 2003). An IMU sensor is low-cost and highly manoeuvrable, but as mentioned in the literature review, is sensitive for drift errors (Chan et al., 2020; Herickhoff et al., 2018a; Rahni & Yahya, 2007). Therefore IMU sensors are often only used in rotation tracking and combined with other translation tracking methods (Chan et al., 2020; Goldsmith et al., 2008; R James Housden et al., 2007). This paper studies the IMU sensors as rotation as well as translation tracking method in 3D ultrasound imaging and compares it with an optical tracking system.

This manuscipt is the first step to study the possibilities of low-cost hand-held 3D ultrasound imaging within the BabyChecker project. The objective is to determine if an IMU sensor can be used as motion tracker in 3D ultrasound imaging using a hand-held ultrasound device.

METHODS

This section is divided into three parts. The first part describes the three steps to create a 3D ultrasound volume: motion tracking, transformation matrix calculation and volume reconstruction. Next, the first experiment is explained, in which the readout of the IMU sensor and the repeatability of the rotation and translation tracking has been studied by moving the IMU sensor over a table. Finally, the second experiment is explained, in which the motion tracking in 3D volume reconstruction of a phantom from the IMU sensor is compared with the optical tracking system.

3D ultrasound reconstruction

The first step in 3D ultrasound reconstruction is 'motion tracking', in which ultrasound images and probe position information is simultaneous acquired. In this study two tracking devices have been used, the smartphone with integrated IMU sensor and an optical tracking system. The smartphone used in this study is a Huawei Nova 5T (version YAL-21), integrated with the lsm6ds3 IMU sensor (Huawei, China). This sensor has been used as motion tracker during the experiments. The optical tracking system is the PST Base HD (PS-tech, Netherlands), this system tracks optical markers attached to the probe with a submillimetre position accuracy and sub-degree rotation accuracy, therefore this system is used as ground truth. The ultrasound probe is the MicrUs Pro C60s (Telemed, Lithuania), which is a convex probe with a depth setting of 20 cm. This probe is connected to the same Huawei smartphone of the IMU sensor. The ultrasound device is operated with an application. After starting a new measurement, by touching the screen of the smartphone, the application records the ultrasound images, accelerometer data and gyroscope data. All recorded data is provided with a timestamp and saved on the phone. The data is acquired using the standard acquisition protocol of BabyChecker, in which a 30 cm sweep is taken in around 5 second with 20 image frames per second. The accelerometer data and gyroscope data are recorded when motion is detected. The accelerometer sensor data is linear interpolated based on the timestamps of the gyroscope in order to have one timestamp for each IMU sensor data. In addition, the initialization of the sensor is corrected, this is explained in appendix 2. All data is analysed in Matlab (Mathworks, Natick, USA).

The second step of 3D ultrasound reconstruction is 'transformation matrix calculation'. In this step the motion tracking data is converted into a transformation matrix. Such a transformation matrix is a combination of a rotation and translation matrix. The calculation method for these matrixes is based on the position estimation algorithm described by Manon Kok (Kok et al., 2017). To transfer the IMU sensor data into a transformation matrix three steps are required: rotation matrix calculation, gravity vector correction and transformation matrix calculation. The first step is to calculate the rotation matrix. Figure 1 shows the dataflow to calculate the rotation matrix, which uses the gyroscope data in Euler angles. In the calculation the earth rotation is neglected. The outcome is a 3x3 rotation matrix which rotate a point consecutively around the x-, y- and z-axis. In the second step the accelerometer data is corrected for the constant present gravitation acceleration of the earth. To obtain solely the acceleration due to movement of to probe, this gravity vector must be removed from the accelerometer data by multiplying an initial gravity vector with the rotational matrix and subtracting this outcome of the corresponding accelerometer data. The initial gravity vector is determined while the phone is hold stable, then the measured acceleration is a combination of noise and the earth gravity. An average is taken over certain measurements to supress this noise. In case the distribution of the measurement values is normal a mean is taken as average, in other cases the median is taken over the values. A Shapiro-Wilk test is used to determine if the distribution is normal (Royston, 1992). In the third step the transformation matrix is calculated, which requires both the gyroscope data and the accelerometer data. In the calculation the gravity corrected accelerometer data is used. The outcome is 1x3 matrix which translates a point over the x-,y- and z-axis. The calculation method for the translation is shown in Figure 2.

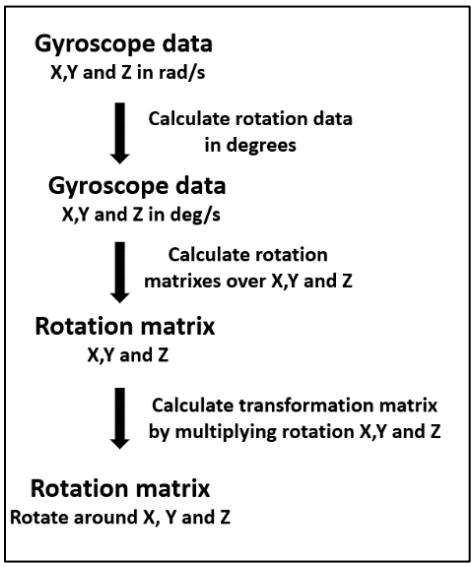

Figure 1. The dataflow of the rotation calculation method.

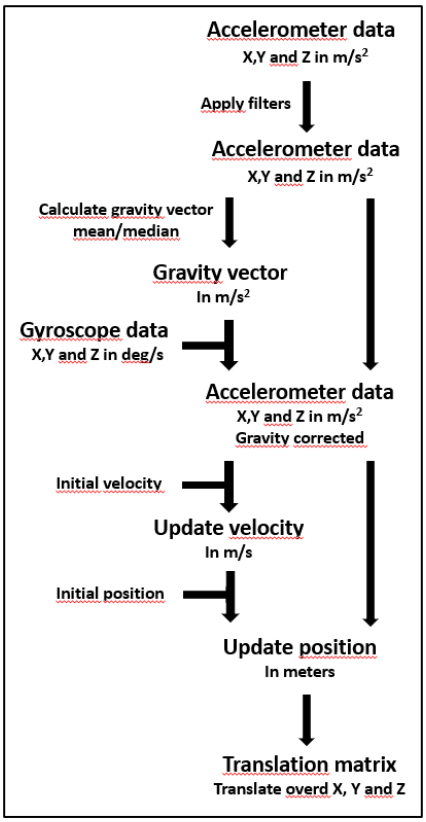

Figure 2. The dataflow of the translation calculation method.

The third step in 3D ultrasound reconstruction is 'volume reconstruction'. In this step the 3D ultrasound volume is reconstructed using the transformation matrix to translate the pixels of the 2D ultrasound images into the voxels of a 3D volume grid. This requires a temporal calibration, spatial calibration and reconstruction step. The first step, 'temporal calibration', aligns the timestamps of the IMU sensor, the optical tracking system and the ultrasound images. This is done by aligning both tracking devices individually with the ultrasound images. The alignment of the IMU sensor and the ultrasound images is done by using the timestamps given to the data by the phone. These timestamps can be directly compared, because both the IMU sensor data and the ultrasound images are stored in the same phone using the same application. The alignment of the IMU sensor and the optical system is done by cross-correlating the movement of the optical tracking system with the movement seen in the ultrasound images while moving the probe up and down in water bath. The method is described in the literature review as 'cross-correlation', see appendix 1. After this temporal calibration step, the positional information of both motion tacking methods have been matched to the ultrasound images. The second step, 'spatial calibration', aligns the coordinates of the ultrasound images with the coordinates of both tracking systems. The spatial calibration is performed with the freehand method using a N-fiducial phantom as described by Carbajal and Chen (Carbajal et al., 2013; Chen et al., 2009). In this method the probe is moved of a phantom with wires in the shape of an horizontal 'N' while the motion is tracked with the optical tracking system. The optical spatial calibration matrix is calculated by using a gradient descent optimalization algorithm to minimize the distances between the coordinates of the wires tracked by the optical system and the coordinates of the wires calculated with the optical transformation matrix multiplied with the spatial calibration matrix and the coordinates of the wires in the ultrasound image. In this study a phantom with three N-fiducials was used and 100 images were manually segmented using 3D Slicer (Fedorov et al., 2012). The optical spatial calibration matrix resulted in a mean offset of 1.1668 +- 0.7925 mm between the reconstructed position of the three wires and the determined position of the three wires with the optical tracking system. The IMU spatial calibration matrix is calculated by matrix

multiplication. Appendix 3 shows the used formulas in the IMU sensor and optical spatial calibration. The third step, ‘reconstruction’, generates a 3D ultrasound volume from the 2D ultrasound images and corresponding position information. To obtain the corresponding position information of the IMU sensor, the phone has been attached to the probe, see Figure 3. The 3D volume is reconstructed by multiplying the transformation matrixes with the corresponding images. Each pixel is translated to a voxel inside a 3D grid. First all the coordinates of the pixels are calculated by multiplying them with the transformation matrix and spatial calibration matrix. Next a 3D grid is generated with sizes based on the outer coordinates of the pixels. This grid is filled with recalculated coordinates of the pixels. The new coordinates are rounded, which results in overwriting a voxel in case two pixels correspond to the same voxel.

Figure 3. This image shows the attachment of the phone to the probe and the optical markers that have been provided to the probe.

Experiment 1. Table

The aim of the first experiment was to test the readout of the IMU sensor in the phone and the repeatability of the motion tracking by moving the phone over a table. The motion has been divided in a rotation and translation movement. A table was chosen because of its flat surface and sharp corners. The rotation and translation measurements where three times repeated to study whether the transformation matrix calculation gives repeatable outcomes.

Experiment 1.1. Rotation

In the rotation measurements the smartphone was three times rotated over three axis. The rotation was 90 degrees and was done by rotating the smartphone by hand over of a table in about 5 seconds. In a 90 degree rotation over the x- and y-axis the corners of the table could be used. The rotation over the z-axis was done by rotating the smartphone along the side of the table. The movements are shown in Figure 4.

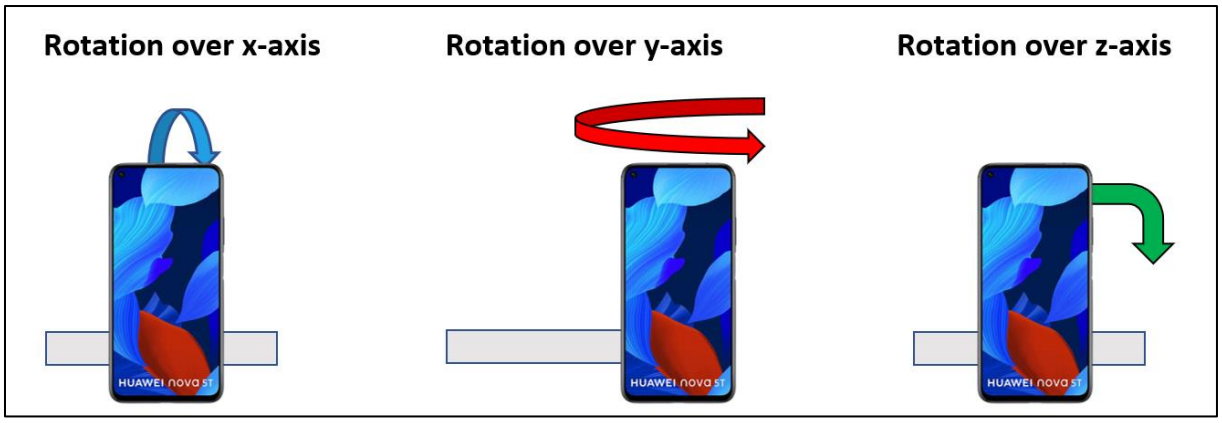

Figure 4. Smartphone movements to assess the rotation performance of the IMU sensor and rotation tracking. In the rotation over the x-axis the phone is tilted backwards, in the rotation over de y-axis the phone is rotated over the corner of the table and in the rotation over de z-axis the phone is moved along the side of the table.

Experiment 1.2: Translation

In the translation measurements the smartphone was three times translated over three axis. The translation was 30 centimetres and was done by translating the smartphone by hand over a table in approximately 5 seconds. This distance and time match the screening protocol of the BabyChecker project, in which the sweeps over the abdomen are 30 cm, taken in 5 seconds. In the x and y movement the tabletop could be used. In the z movement the smartphone was pushed against a box and moved over the table in that way, the box was used to give the smartphone more stability compared to a freehand translation. The movements are shown in Figure 5.

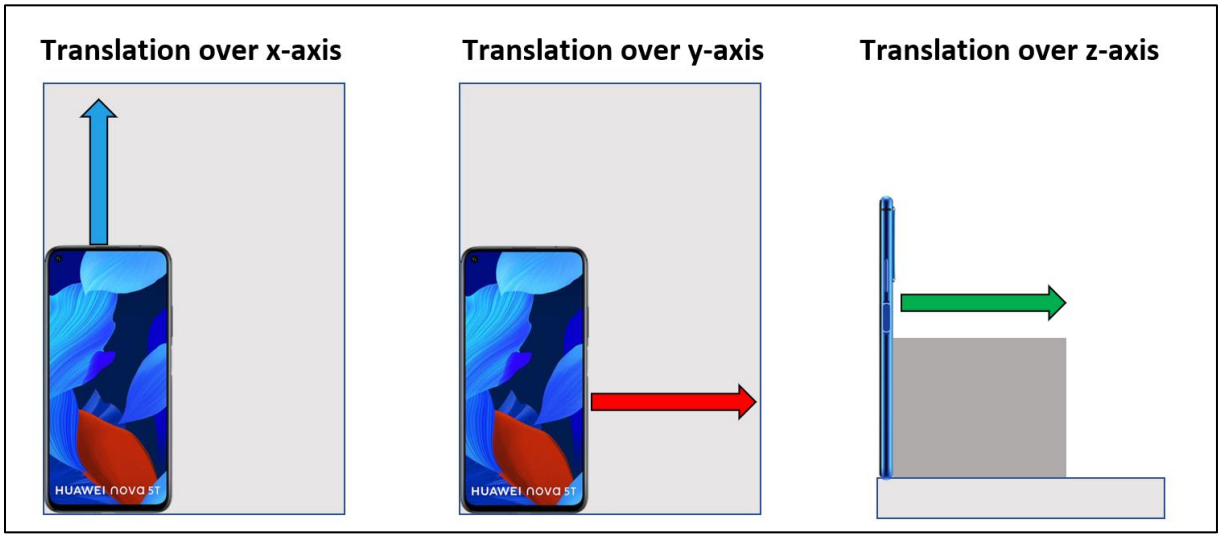

Figure . Smartphone movements to assess the translation performance of the IMU sensor and transformation calculation method. In the translation over the x- and y-axis the phone is moved over the table and in the translation over de z-axis the phone is pushed against a box and moved over the table in that way.

Experiment 1.2.1. Gravity vector

As explained, in the second step of 3D ultrasound reconstruction, 'transformation matrix calculation', the gravity vector is important, because the accelerometer data needs to be corrected for this vector. An initial gravity vector is determined when the probe lies stable and therefore only measures the earth gravity with noise. This initial gravity vector is thereafter subtracted from the accelerometer data using the rotation matrix to determine the orientation of the phone. In this study

four different gravity calculation methods have been used to test the influence of the initial gravity vector on the translation tracking. All calculation methods use data in which the probe was held stable during the first second. A delay of 0.5 seconds has been chosen to exclude possible vibrations due to starting the measurement by touching the phone. The calculation methods are:

1. The first single value of the accelerometer data readout of the x-,y- and z-axis;
2. the first single value of the accelerometer data readout of the x-,y- and z-axis after 0.5 seconds;
3. the average value of the accelerometer data of the x-,y- and z-axis between 0 and 1 seconds;
4. the average value of the accelerometer data of the x-,y- and z-axis between 0.5 and 1 seconds.

Experiment 1.2.2. Accelerometer data filtering

As mentioned in the introduction, the translation tracking with an IMU sensor suffers from drift errors (Chan et al., 2020; Herickhoff et al., 2018a; Rahni & Yahya, 2007). Filters have been applied to the accelerometer data to study the effect on suppressing these drift errors. Five different filters have been applied to the raw accelerometer data to test if it would increase the repeatability of the translation tracking. The filters that have been used are:

1. outlier filter, which filters the data of sudden tremors and removes data that lies more than 1.5 interquartile range above the upper quartile or below the lower quartile of the dataset;
2. low-pass filter: which filter the data of high frequency signal changes and uses a cut off frequency of arbitrarily chosen 10 Hz, assuming the acceleration is not rapidly changing;
3. moving mean: which filters the data of white noise and takes the mean value over arbitrarily chosen 11 and 41 measurements;
4. quadratic Savitzky-Golay: which filters the data of noise, but maintains peaks in the data, the filter length is arbitrarily chosen 11 and 41 measurements, the reader is referred to Schafer for more information about Savitzky-Golay filtering (Schafer, 2011);
5. cubic Savitzky-Golay: which filters the data of noise, but maintains peaks in the data, the filter length is arbitrarily chosen 11 and 41 measurements.

Experiment 2. Phantom

The aim of the second experiment was to assess the IMU sensor in motion tracking for 3D ultrasound reconstruction of a phantom by comparing it with the optical tracking system. The IMU sensor was assessed in three experiments, which are repeated for the rotation and the translation movement separately. First, the motion tracking of the IMU sensor was compared with the optical system. Second, a comparison was made between the cross-sectional plane of a reconstructed 3D ultrasound volume from the motion tracking of an IMU sensor and an optical system. Third, the distance between phantom features in both reconstructed volumes are calculated. The phantom is the Multipurpose Ultrasound Phantom ATS 539, shown in Figure 6. The phantom has been placed along the z-axis of the optical tracking system, this has been done by eye.

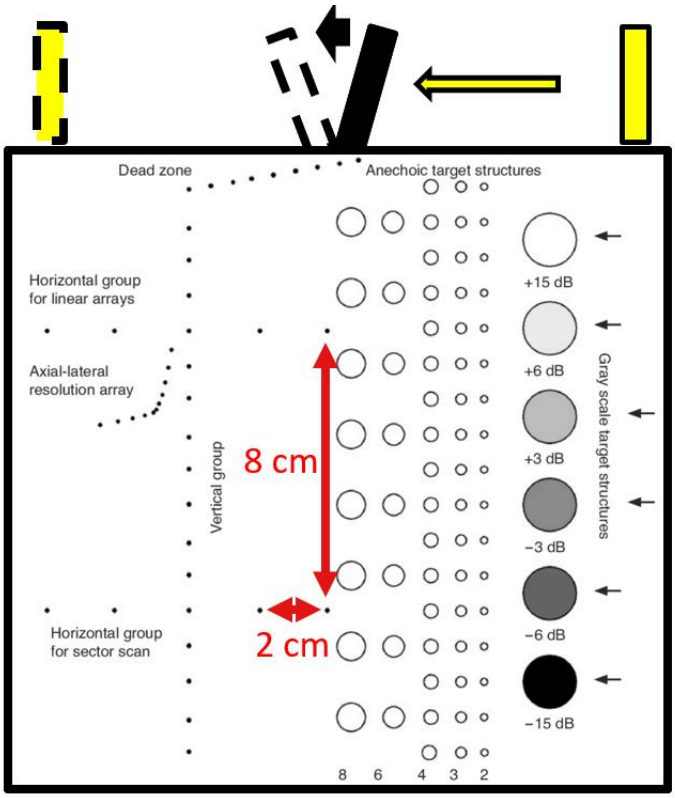

Figure 6. The multipurpose Phantom ATS 539. The two distance have been used in the distance-based accuracy experiments. In black and yellow the positions of the ultrasound probe during respectively rotation and translation movements are shown.

Experiment 2.1. Rotation

In the rotation experiment the probe was rotated 40 degrees by hand over the phantom at the location shown in Figure 6. The rotation was limited to 40 degrees, because there has to be a line of sight between the optical tracking system and the optical markers. The scanning protocol was as followed. First the optical tracking system was temporal calibrated. Secondly, the probe was moved to the initial position and held stable for approximately 2 seconds. The probe is held under an angle of approximately -20 degrees which is taken as zero degrees in both the IMU sensor as the optical tracking system. Thirdly, the probe is rotated 40 degrees in 2.5 seconds. Lastly, the probe was moved back to the initial position and the movement was repeated twice. In postprocessing, the temporal calibration and measurements are manually selected and processed separately.

Experiment 2.1.1. Motion tracking

First, the rotation and translation movements of the IMU sensor are compared with the optical tracking system by calculating the Pearson's correlation coefficient. In addition, the effect of choosing a different start is studied by shifting the start of the rotations calculated with the IMU sensor by one frame. By interpolation, this frame shift corresponds to a shift of approximately ten sensor data points.

Experiment 2.1.2. Reconstruction of 3D ultrasound volume

Secondly, the cross-sectional planes of both an IMU sensor and an optical system reconstructed 3D volume are compared. In the optical reconstruction the whole transformation matrix was taken, including all rotations and translations. The IMU sensor reconstruction has been performed with only the rotations.

In both reconstructions the volumes have been filled with a morphological opening algorithm. This algorithm first fills the empty voxels inside an ultrasound image and continuous with the other empty voxel by using a rectangular averaging kernel of 11x11.

Experiment 2.1.3. Distance-based accuracy

Thirdly, two distances between phantom features have been calculated, the distances are shown in Figure 6. To determine the distances, four phantom features have been manually selected in the ultrasound images. The coordinates of these datapoints are transformed with the corresponding optical tracking and IMU sensor transformation matrix to obtain the coordinates of the points inside the 3D volume. Subsequently, the distances between the coordinates of the points within the 3D volume have been calculated.

Experiment 2.2. Translation

In the translation experiment the probe was translated 15cm by hand over the phantom at the location shown in Figure 6. The scanning protocol was as followed. First the optical tracking system was temporal calibrated. Secondly, the probe was moved to the initial position on the left side of the phantom and held stable for 2 seconds. Thirdly, the probe was moved to the right side of the phantom in 2.5 seconds. At last, the probe was held stable again. The movement over the phantom was repeated twice. In postprocessing, the temporal calibration and measurements are manually selected and processed separately.

Experiment 2.2.1. Motion tracking

First, the rotation and translation movements of the IMU sensor are compared with the optical tracking system by calculating the Pearson's correlation coefficient. In addition, the effect of choosing a different start is studied. The start of the translations calculated with the IMU sensor is shifted with respectively one frame, because of interpolation this frameshift corresponds to a shift of approximately ten sensor datapoints. Taking a different start results in a different initial gravity vector.

Experiment 2.2.2. Cross sectional plane

Secondly, a cross-sectional plane of an IMU sensor reconstructed 3D volume is compared with an optical reconstructed 3D volume. In the optical reconstruction the whole transformation matrix was taken, including all rotation and translation motions. The IMU sensor reconstruction has been performed with all the rotation motions and only the translation motion over the z-axis.
In both reconstructions the volumes have been filled with a morphological opening algorithm. This algorithm first fills the empty voxels inside an ultrasound image and continuous with the other empty voxel by using a rectangular averaging kernel of 11x11.

Experiment 2.2.3. Distance-based accuracy

Thirdly, two distances between phantom features have been calculated, the distances are shown in Figure 6. To determine the distances, four phantom features have been manually selected in the ultrasound images. The coordinates of these datapoints are transformed with the corresponding optical tracking and IMU sensor transformation matrix to obtain the coordinates of the point inside the 3D volume. Subsequently, the distances between the coordinates of the points within the 3D volume are calculated.

RESULTS

This section shows the results of the two experiments that were performed. In the first experiment the IMU sensor was moved over a table. In the second experiment the IMU sensor motion tracking was compared to the optical system while moving the probe over a phantom.

Experiment 1. Table

In the first experiment the smartphone, with integrated IMU sensor, was rotated and translated over a table to test the readouts of the IMU sensor and the repeatability over the motion tracking.

Experiment 1.1. Rotation

In the rotation experiment the smartphone was rotated 90 degrees during approximately 5 seconds, the results are shown in Figure 7. The measurements show a repeatable result in which the start, motion and end of the experiment can be clearly distinguished. The average measured rotation over the x-axis is 90 degrees, over the y-axis is -88 ± 0.13 degrees and over the z-axis is 94 ± 1.7 degrees.

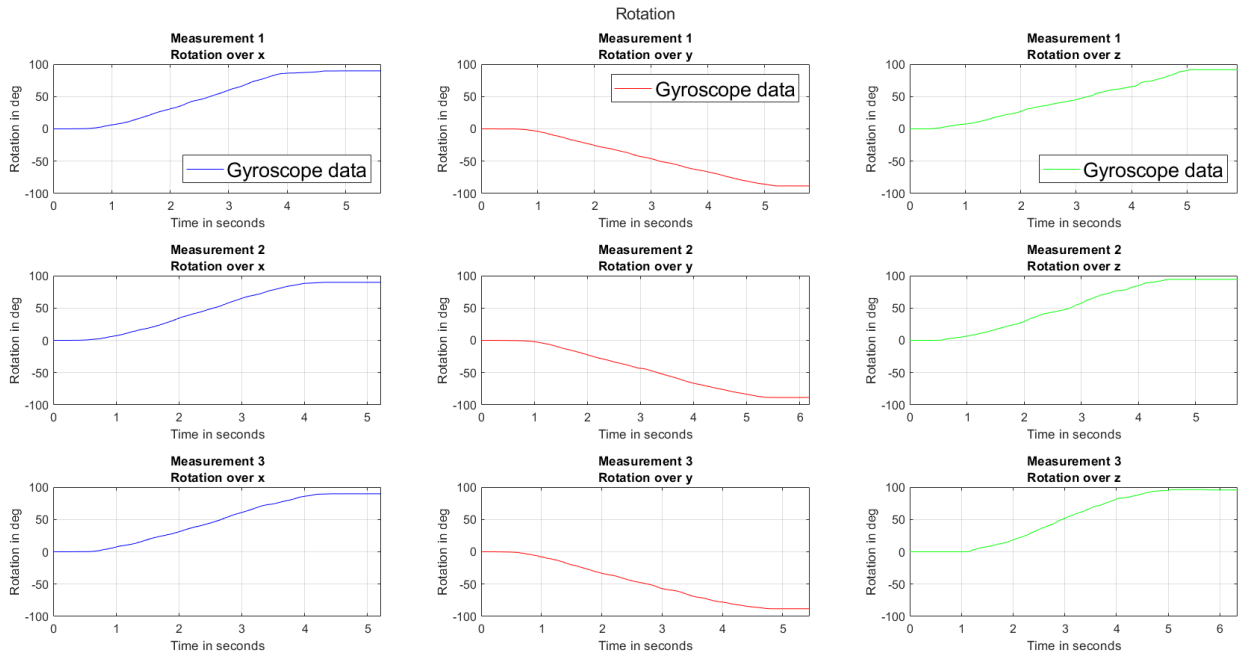

Figure 7. The rotation estimation of the IMU sensor while rotating 90 degrees.

Experiment 1.2. Translation

In the translation experiment the smartphone is 30 cm translated during approximately 5 seconds, in accordance to the screening protocol of the BabyChecker project. The effect of the gravity vector and accelerometer data filtering has been studied in two separate experiments, the results are shown below.

Experiment 1.2.1. Gravity vector

The effect of four different initial gravity vector calculation methods on the translation tracking has been studied. The different calculation methods result in a different gravity vector. These difference in the gravity vector highly influence the repeatability of the translation tracking method as can be seen in Figure 8. The average translation by taking the first value is 160 ± 200 cm, by taking the first value after 0.5 second is 41 ± 33 cm, taking the average between 0 and 1 second is 28 ± 18 cm and by taking the average value between 0.5 and 1 second is 26 ± 20 cm. The results can be explained by the accelerometer data. When the probe is stable, the accelerometer data is a combination of the gravity vector and noise. Choosing a single measurement value as gravity vector, the translation can be

affected with a drift error. Taking an average does repress this drift error, however doesn't always give a good result. Another source of error are vibrations which occur when the phone is touched as the start of a measurement. Concluding, the best initial gravity vector has been chosen to be a calculation of the average over the measurements between 0.5 and 1 second. This value has been used throughout the study.

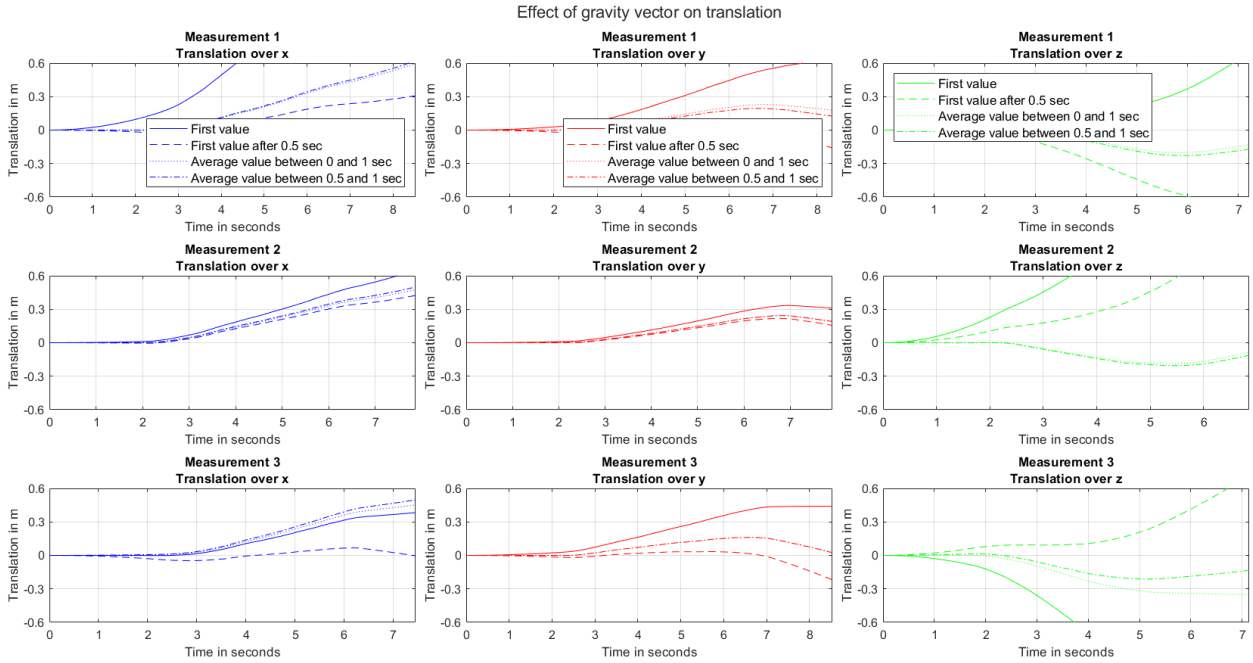

Figure 8. The effect of the gravity vector on the translation estimation of the IMU sensor while translating approximately 0.3 meter, the graphs respectively show a gravity vector based on a) the first measurement value, b) the first measurement after 0.5 seconds, c) the average measurement values between 0 and 1 second and d) the average measurement between 0.5 and 1 second.

Experiment 1.2.2. Accelerometer data filtering

In an attempt to improve the translation tracking, the effect of five filters on the raw accelerometer data has been studied. The result of the translation tracking after filtering is shown in Figure 9. In this experiment the initial gravity vector is the average value of the measurements between 0.5 and 1 second. Unfortunately, none of the filters resulted in an improvement of the translations. The outlier filter does improve some of the measurement, but made the translation tracking in other measurements worse.

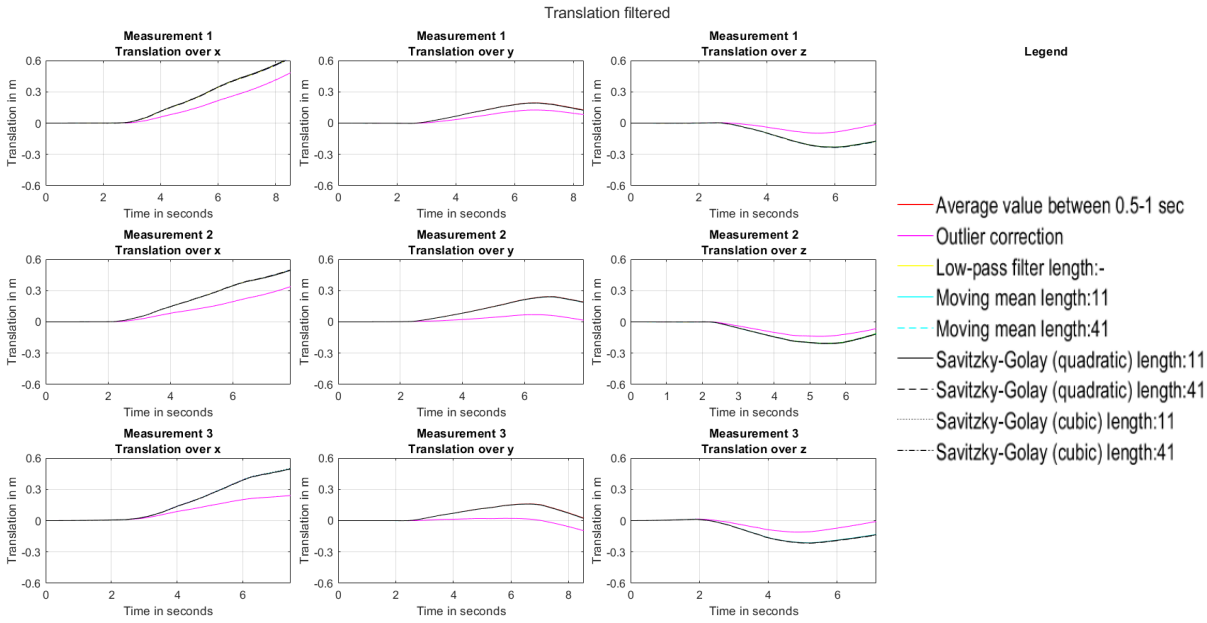

Figure 9. The effect of different filters on the translation estimation of the IMU sensor while translating approximately 0.3 meter, the data is a gravity corrected using the average between 0.5 and 1 second as gravity vector. The filters are respectively: outlier, low-pass, moving mean (frame length 11 & 41), cubic Savitzky-Golay (frame length 11 & 41) and quadratic Savitzky-Golay (frame length 11 & 41).

Experiment 2. Phantom

In the second experiment, the IMU sensor was compared with an optical tracking system while rotating and translating over a phantom. The aim of this experiment was to test the IMU sensor by comparing the motion tracking with the optical system and by comparing a reconstructed 3D ultrasound volume. The comparison is made in three sub-experiments for rotation and translation movement each: motion tracking, cross sectional plane and distance-based accuracy.

Experiment 2.1 Rotation

In the rotation movement the probe was rotated 40 degrees in 2.5 seconds. The movement of the IMU sensor is compared to the same movement tracked by the optical system. In Figure 10 the rotation and translation motions of the first rotation measurement is shown. While rotating over the x-axis the other rotation parameters are accurate as well. However, the translation parameters are effected by a drift error resulting is large discrepancy between the optical tracking system and the IMU sensor. Therefore, the rotation accuracy is determined with solely the rotational parameters of the IMU sensor compared with the rotation and translation parameters of the optical tracking system.

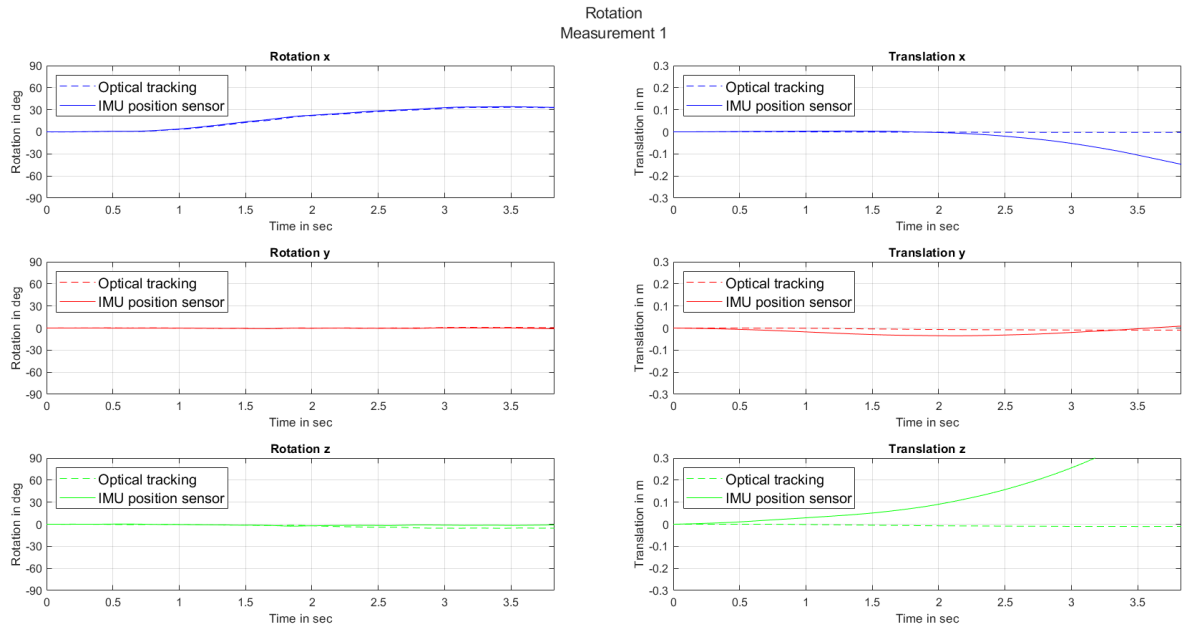

Figure 10. The rotation and translation movements of the IMU sensor compared with optical tracking system while rotating over the x-axis.

Experiment 2.1.1. Motion tracking

The motion of the rotation over the x-axis is shown in Figure 11. The IMU sensor rotations are calculated with several starting position, which do not significantly affect the rotation. Any outlier in the optical tracking system is a result of a loss in the line of sight between the optical tracking system and the optical markers. The Pearson's correlation coefficient is calculated to compare the motion tracking of the IMU sensor and the optical system. The average correlation in measurement 1 is 1.0 ± 4.3E-06, in measurement 2 is 0.98 ± 9.4E-04 and in measurement 3 is 1.0 ± 3E-06.

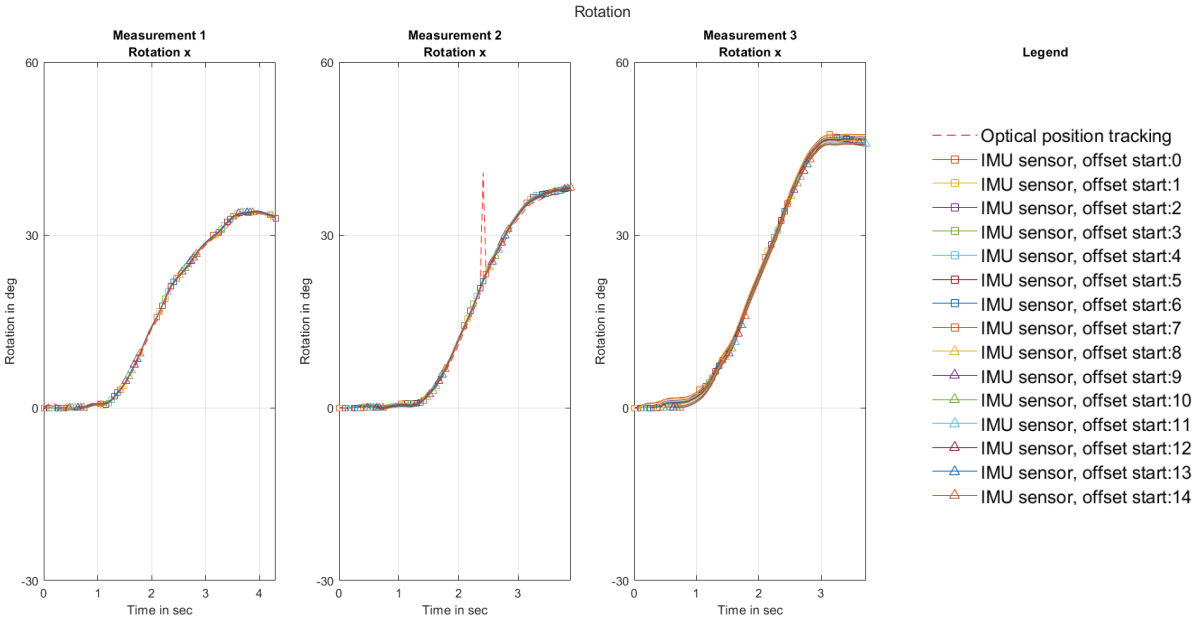

Figure 11. The effect of using different starting points in the rotation estimation of the IMU sensor compared with the optical tracking system while rocking over the phantom.

Experiment 2.1.2. Cross sectional plane

The cross sectional planes of the IMU sensor and optical system reconstructed 3D volumes of measurement 1 are shown in the figures 12 till 15. These cross sectional planes are shown to assess the performance of the IMU sensor in reconstructing a 3D volume. As can be seen in the Figure 12 and 13, respectively IMU sensor and optical system reconstructthe volumes are sparsely filled which makes it difficult to compare. In figure 14 and 15 the same cross sectional planes are shown after the volumes are filled with a morphological opening.

The phantom features in the IMU sensor reconstructed 3D volume look the same as in the optical reconstructed 3D volume. This is also expected, based on the high correlation of the motion tracking.

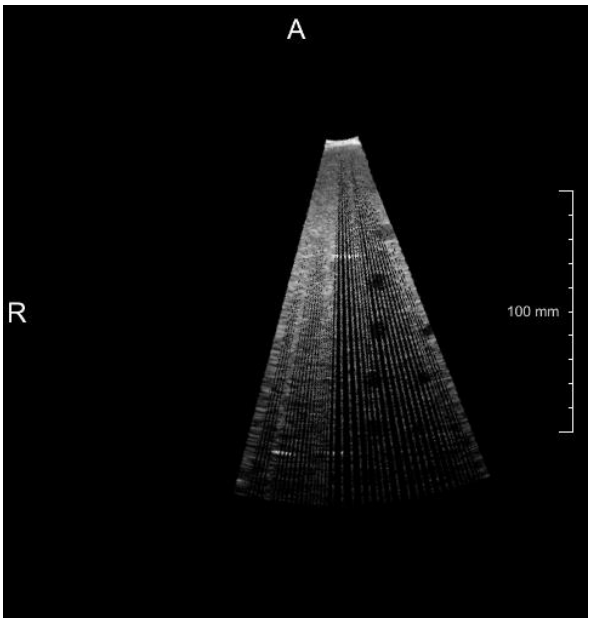

Figure 12. A cross sectional plane of the reconstructed 3D volume of a rotation over the phantom using the IMU sensor transformation matrix.

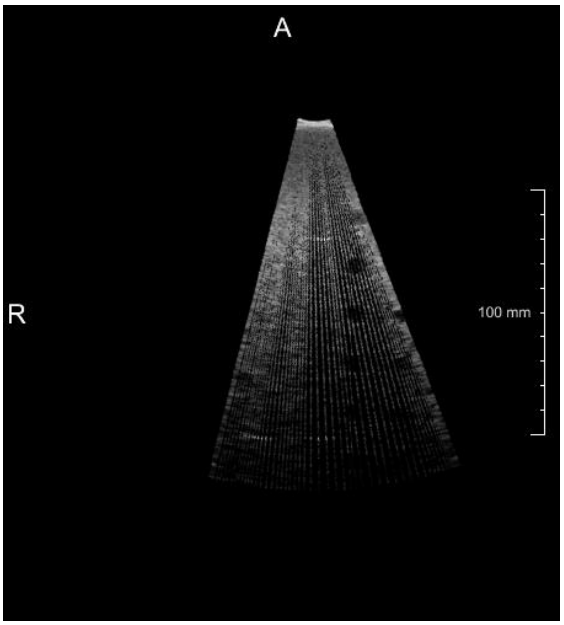

Figure 13. A cross sectional plane of the reconstructed 3D volume of a rotation over the phantom using the optical tracking transformation matrix.

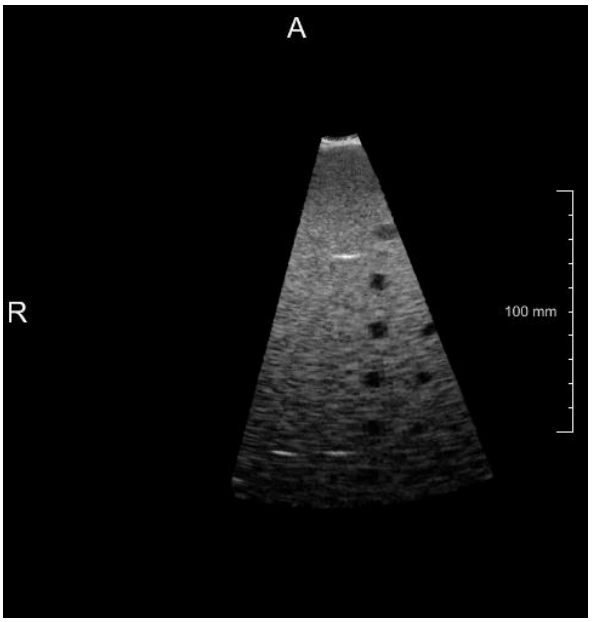

Figure 14. A cross sectional plane of the filled reconstructed 3D volume of a rotation over the phantom using the IMU sensor transformation matrix.

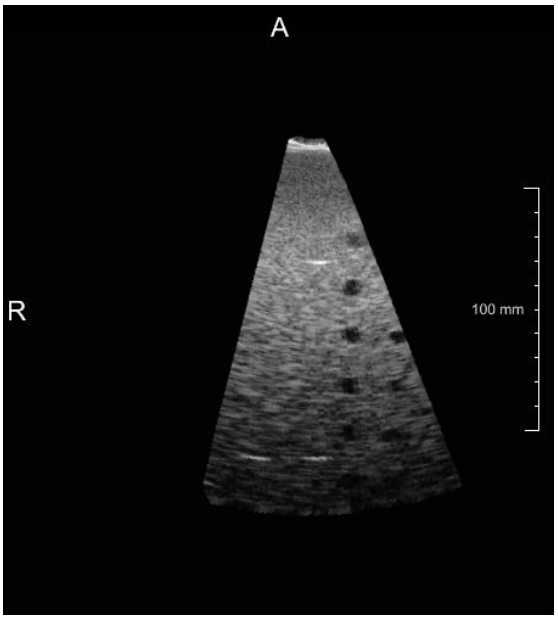

Figure 15. A cross sectional plane of the filled reconstructed 3D volume of a rotation over the phantom using the optical tracking transformation matrix.

Experiment 2.1.3. Distance-based accuracy

The last experiment calculates the distances-based accuracy between phantom features in the rotation based reconstructed volumes. The used phantom features and distances are shown in Figure 6. The results are shown in table 1 and 2, respectively vertical and horizontal distances in the phantom.

Experiment 2.1.3. Rotation, distance-based accuracy in vertical direction			
	Measurement 1	Measurement 2	Measurement 3
Optical tracking (cm)	8.11	8.11	8.07
IMU sensor (cm)	8.15	8.12	8.08
Absolute difference (cm)	0.04	0.01	0.01
Relative difference (%)	0.407	0.187	0.167

Table 1: The vertical distance between two wires in the 3D reconstructed volumes of a rotation over the phantom. The distance between the wires in the phantom itself is 8cm.

Experiment 2.1.3. Rotation, distance-based accuracy in horizontal direction			
	Measurement 1	Measurement 2	Measurement 3
Optical tracking (cm)	2.11	1.93	2.02
IMU sensor (cm)	0.86	1.17	1.28
Absolute difference (cm)	1.25	0.76	0.74
Relative difference (%)	59.2	39,5	36.7

Table 2: The horizontal distance between two wires in the 3D reconstructed volumes of a rotation over the phantom. The distance between the wires in the phantom itself is 2cm.

Experiment 2.2. Translation

In the translation experiment the probe was translated 15 cm in 2.5 seconds. The motion of the IMU sensor is compared to the same motion tracked by the optical system. In Figure 16 the rotation and translation movements of the second measurement are shown. As can be seen, the rotations of the IMU and the optical tracking are aligned. However, the translations over the x- and y-axis are

effected by a drift error, resulting in a discrepancy between the optical tracking system and the IMU sensor. Therefore, the rotational parameters and only the z-axis translation of the IMU sensor was compared with all rotations and translations of the optical tracking system.

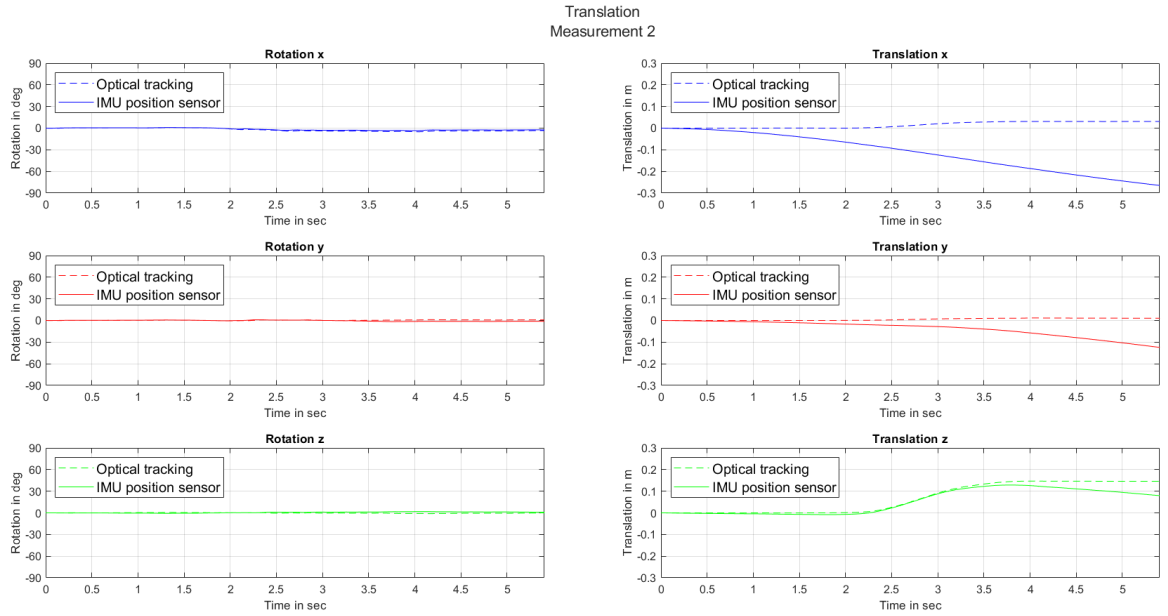

Figure 16. The rotation and translation movements of the IMU sensor compared with optical tracking system while translating over the z-axis.

Experiment 2.2.1. Motion tracking of an IMU sensor versus an optical system

The translation tracking of a translation over the z-axis is shown in Figure 17. The IMU sensor translation tracking is calculated with several starting position, which do significantly affect the motion. Some motions of the IMU sensor are closely aligned with those of the optical tracking system. Choosing a different start position results in a different gravity vector and different rotation and acceleration values at the start of a measurement. To compare the motion tracking the Pearson's correlation coefficient is calculated. The average correlation in measurement 1 is 0.40 ± 0.72, in measurement 2 is 0.14 ± 0.73 and in measurement 3 is 0.16 ± 0.78.

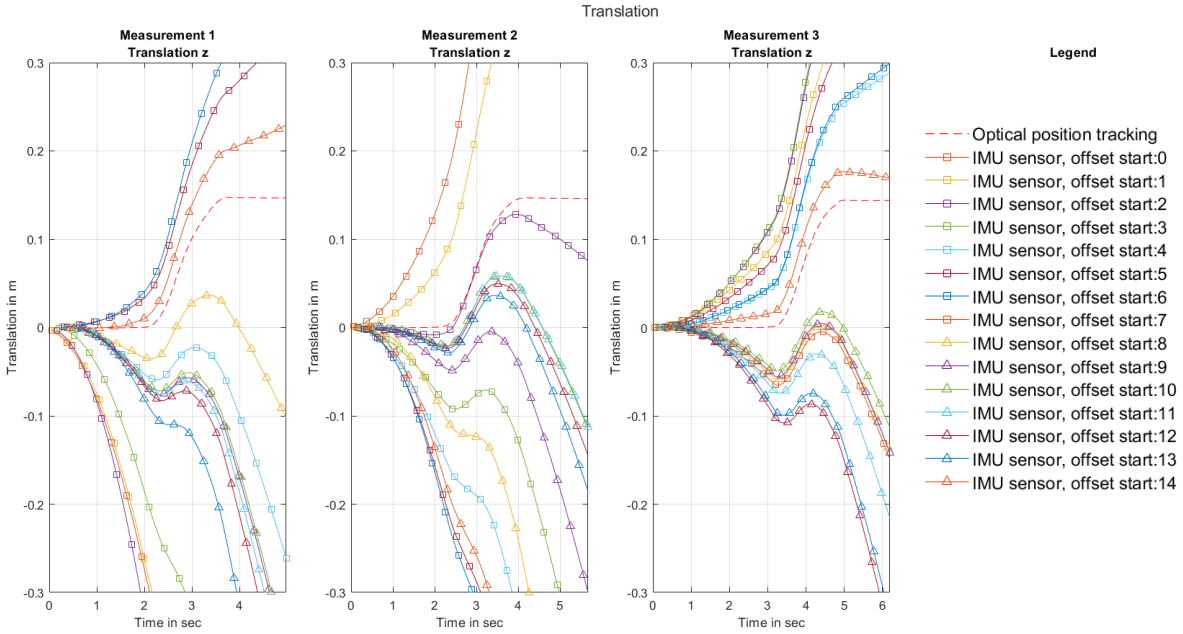

Figure 17. The effect of using different starting points in the rotation estimation of the IMU sensor compared with the optical tracking system while rocking over the phantom.

Experiment 2.2.2. Cross sectional plane

The cross sectional planes of the IMU sensor and optical system reconstructed 3D volumes of measurement 2, with IMU sensor start 2, are shown in the figures 18 till 22. The cross sectional planes are shown to assess the performance of the IMU sensor in reconstructing a 3D volume. As can be seen in the Figure 18 and 19, , respectively IMU sensor and optical system reconstruction, the volumes are sparsely filled which makes it difficult to compare both reconstructions. In figure 20 and 21, respectively IMU sensor and optical system reconstruction, the same cross sectional planes are shown after the volumes are filled with a morphological opening. These figures show that at the end of the IMU sensor reconstructed volume the images are positioned backwards of the probe movement, this is in line with what you expect based on the measurement motion.

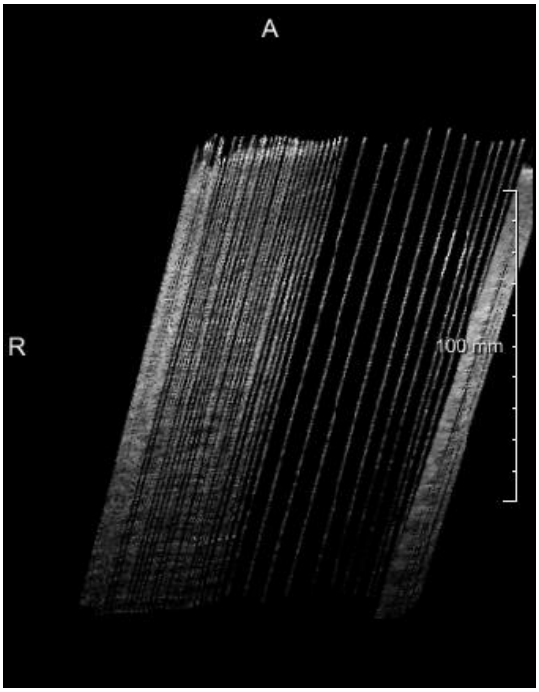

Figure 18. Cross-sectional plane of a reconstructed 3D volume of a translation using a IMU sensor based transformation matrix.

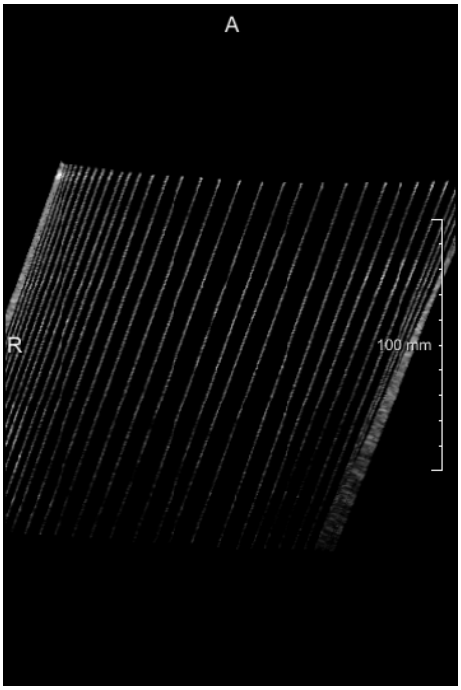

Figure 19. Cross-sectional plane of a reconstructed 3D volume of a translation using an optical tracking based transformation matrix.

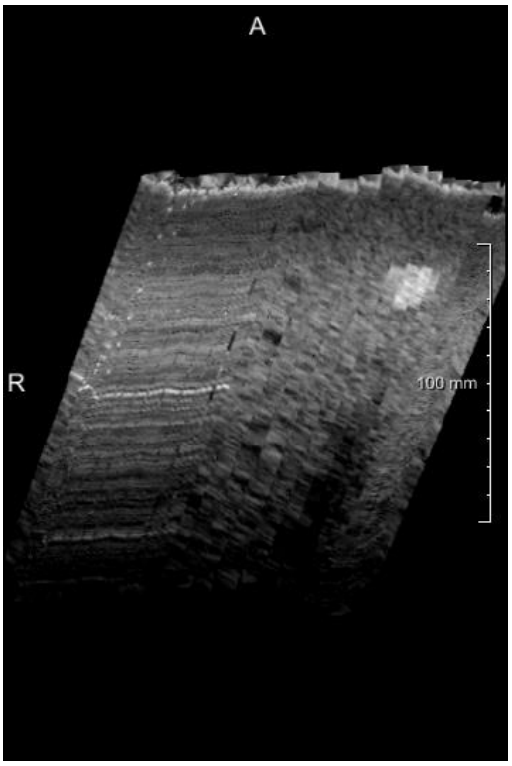

Figure 20. Cross-sectional plane of a filled reconstructed 3D volume of a translation using a IMU sensor based transformation matrix.

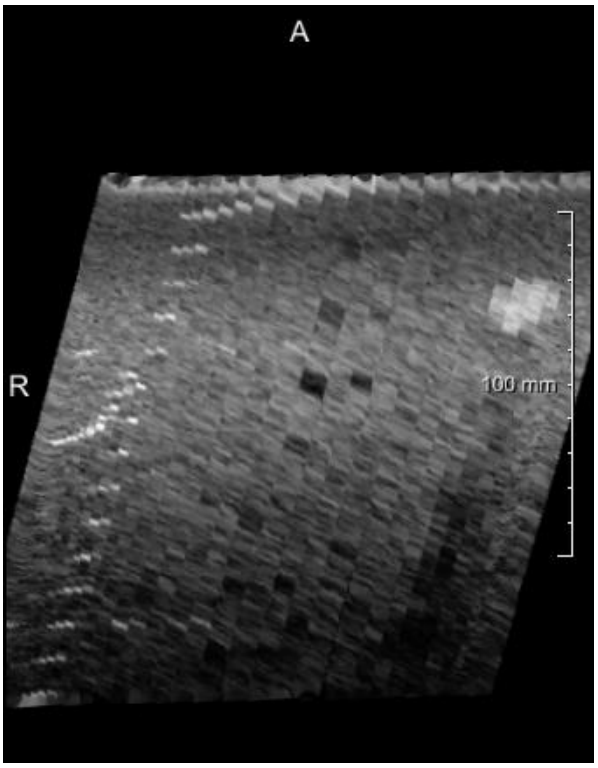

Figure 21. Cross-sectional plane of a filled reconstructed 3D volume of a translation using an optical tracking based transformation matrix.

2.2.3. Distance-based accuracy

The last experiment calculates the distances between phantom features in the translation based reconstructed volumes. The used phantom features and distances are shown in Figure 6. The results are shown in table 3 and 4, respectively vertical and horizontal distances in the phantom.

Experiment 2.2.3. Translation, distance-based accuracy in vertical direction			
	Measurement 1	Measurement 2	Measurement 3
Optical tracking (cm)	8.23	6.14	8.20
IMU sensor (cm)	8.16	6.31	8.23
Absolute difference (cm)	0.07	0.17	0.03
Relative difference (%)	0.924	2.75	0.456

Table 3: The vertical distance between two wires in the 3D reconstructed volumes of a translation over the phantom. The distance between the wires in the phantom itself is 8cm.

Experiment 2.2.3. Translation, distance-based accuracy in horizontal direction			
	Measurement 1	Measurement 2	Measurement 3
Optical tracking (cm)	1.79	1.99	2.95
IMU sensor (cm)	3.14	2.01	2.64
Absolute difference (cm)	1.35	0.02	0.31
Relative difference (%)	75.7	1.38	10.6

Table 4: The horizontal distance between two wires in the 3D reconstructed volumes of a translation over the phantom. The distance between the wires in the phantom itself is 2cm.

DISCUSSION

The aim of this study was to develop a method for low-cost 3D ultrasound which can be used within the BabyChecker project. As low-cost 3D ultrasound reconstruction method the motion tracking of an IMU sensor has been tested and compared with an optical tracking system. The motion has been divided in a rotation and a translation movement. The rotation tracking of the IMU sensor showed to give repeatable and similar results as the optical tracking system. The translation tracking with an IMU sensor showed to be not repeatable or comparable to the optical tracking system. The driving factor in the IMU sensor translation tracking results is the initial gravity vector, as shown in experiment 1.2.1 and experiment 2.2.1.

Experiment 1. Table

In experiment 1 the readout of the IMU sensor and the repeatability of the rotation and translation tracking of the IMU sensor has been studied, by moving a smartphone with integrated IMU sensor over a table. In experiment 1.1 the rotation tracking showed to give repeatable results in which the start, motion and end of the smartphone movement can be distinguished. The smartphone was rotated around 90 degrees and as calculated in experiment 1.1.1 the average IMU sensor rotation tracking was 90 ± 2.6 degrees. In experiment 1.2.1 and 1.2.2 the translation tracking showed to give a large measurement variation. In experiment 1.2.1 the effect of four different initial gravity vectors calculation methods on the translation tracking has been studied. In this experiment the smartphone was moved 30 cm over a table, the distance had been determined with a ruler which introduce a deviation of 2 cm. Four initial gravity vector calculation methods have been used: a) the first measurement value ,b) the first measurement value after 0.5 seconds, c) the average measurement value between 0 and 1 second and d) the average measurement value between 0.5 and 1 second. All these method had a large measurement variability, respectively 160 ± 200 cm, 41 ± 33 cm, 28 ± 18 cm and 26 ± 20 cm. Taking an average improves the tracking result significantly, because the noise of the accelerometer data is suppressed. Filtering of the accelerometer data did not improve the results, as shown in experiment 1.2.2.

Experiment 2. Phantom

In experiment 2 the movement of the IMU sensor is compared with the optical tracking system. In this experiment the phone is attached to the probe using cable wires. In experiment 2.1.1 the rotation tracking of the IMU sensor and the optical system are compared, they show a similar motion with an average Pearson's correlation of 0.99 ± 0.0056. This correlation indicates a good accuracy of the IMU sensor rotation tracking. In experiment 2.1.2 the cross-section planes of a IMU sensor and optical tracking system reconstructed phantom volume are compared. The planes of the IMU sensor and the optical system in the reconstructed volume show similar phantom features. In experiment 2.1.3 the distance-based accuracy between phantom features is measured. Between vertical phantom features the average error is 45% and between horizontal features the error is 0.25%. Based on the similarity in the motion tracking such an error is not expected. The error may have occurred due to the absence of the translation matrix or due to the elevation beam focus, further explained in the research limitations below. In experiment 2.2 the translation tracking of the IMU sensor was compared with the optical tracking system. In experiment 2.2.1 the average Pearson's correlation over the translation was 0.13 ± 0.78. This experiment shows that the IMU sensor has a bad performance in translation tracking compared with the optical system. Although the correlation is weak, in some translations the end, motion and stop showed similarity. One of the reasons of a weak correlation is the initial gravity vector. Using a different initial gravity vector, by changing the start of the measurement, the translations differ greatly. In experiment 2.2.2 the cross sectional planes are shown of a volume reconstructed after a translation over the phantom. The cross sectional planes are skewed due to the setup in which the optical system measures the probe with

optical markers under an angle. In the cross sectional planes the phantom features are difficult to compare, because the images are sparsely filled and hence blurred in the filled reconstruction. The relative distance-based accuracy measurement of experiment 2.2.3. gives an average error of 29% in the vertical direction and an error of 1.4% in the horizontal direction.

Research limitations

In this research four major limitations have been identified: the phone attachment to the probe, the absence of translation parameters in the volume reconstruction, the elevational beam focus in the ultrasound images and the number of images per distance.

The first limitation is the attachment of the phone to the probe. This fixture must be rigid and minor movements may have occurred with the current method of cable wires. Although this fixture was not completely rigid, the IMU sensor rotation tracking was repeatable and accurate, indicating that the movements within the fixture were small.

The second limitation is the absence of translation parameters in the reconstruction of the 3D ultrasound volume with the IMU sensor motion tracking. The ultrasound volume reconstruction with optical tracking is a combination of rotation and translation tracking. This full translation matrix has been compared with only the rotation tracking in experiment 2.1.2 and the rotation tracking plus translation over the z-axis in experiment 2.2.2 This way of comparing introduces an error between the optical tracking and the IMU sensor.

The third limitation is the elevational beam focus which can partly explain the outcomes in the distance based accuracy measures. Within the volume reconstruction of a rotation, experiment 2.1.2, three lines can be seen at the left, which should have appeared as dots. These lines may have occurred due to elevational beam focus, which makes it hard to distinguish the phantom features from scattering. The corresponding relative distance-based measure in the vertical direction of experiment 2.1.3 shows good results, however, because this is an in-plane distance it is not a good representation of a 3D volume reconstruction. The relative difference in the horizontal direction of experiment 2.1.3 has a large error, which can be due to this elevational beam focus and also due to the lack of the translation movement of the IMU sensor. The same reasoning can be applied to translation volume reconstruction of experiment 2.2.2 and 2.2.3.

The last limitation is the number of images per distance, which is the reason why the 3D reconstructed volumes are sparsely filled. To obtain more images per distance two adjustment could be made. The first adjustment is to lower the motion speed of the probe. Since this study is part the BabyChecker project the motion speed of the probe movement was restricted to 6 centimetres per centimetres, according to the scanning protocol of 30 centimetres in 5 seconds. Another adjustment is to increase the image sampling frequency within the ultrasound image acquisition.

Future research

This study tested the IMU sensor as motion tracker for the reconstruction of 3D ultrasound volumes from 2D ultrasound sweeps over the abdomen of pregnant women. A translational research step must be made to assess the motion tracking of IMU sensors in this clinical setting. The presented method for rotation tracking with the IMU sensor showed repeatable and accurate results and follow-up research can study the rotation tracking in the clinic. A clinical evaluation should indicate whether a rocking motion has a sufficient field of view to screen the fetus and in what extend movements of the women and the fetus affect the result. The presented method for translation tracking with the IMU sensor requires addition research on the initial gravity vector before a clinical evaluation study can be performed. As mentioned in the literature review, motion tracking with IMU sensors is sensitive for drift errors and therefore IMU sensors are often only used in rotation tracking in combination with other translation tracking methods, see appendix 1. Follow-up research can study if other motion tracking methods outperform the IMU sensor in translation tracking.

CONCLUSION

This study showed the motion tracking of an IMU sensor in comparison with an optical tracking system. The motion has been divided into a rotation and translation movement. The rotation tracking of the IMU sensor showed to give repeatable and similar results as the optical tracking system. The translation tracking of the IMU sensor has shown to be not repeatable or comparable to the optical tracking system. The driving factor in the translation tracking results is the initial gravity vector which is used for gravity vector correction in the accelerometer data. Future research should focus on the clinical evaluation of the rotation tracking and the development of accurate translation tracking by studying the initial gravity vector or looking at different translation tracking methods.

ACKNOWLEDGEMENT

This master's thesis presents my graduation research on the topic of three-dimensional ultrasound during the period from June 2020 to March 2021. These months have been very educational in both a personal and scientific way, for which I would I want to express my gratitude to the people who helped me along the way.

I want to thank my supervisors Thomas van den Heuvel and Nandini Bhattacharya for guiding me through the research in the unpredictable times of a global pandemic. I want to thank Thomas for providing me this opportunity, his problem solving during the project and providing me feedback from where I could continue to learn. I want to thank Nandini for her support during the past months, which helped me to stay focused and positive throughout the work.

A special thanks to the MUSIC research group for providing me feedback during the project and for the warm welcome. Although we as group could not meet often, I always felt that I could easily get in contact and have a nice conversation. In particular I would like to thank Anton Nikolaev for the fruitful co-operation and discussions on many different issues. The enthusiasm of Anton was very motivating during the project.

My dear thanks to my family and friends for their patience and welcome distraction from studying on the weekends and evenings, in particular to Hans, Alja, Sander, Dunja, Bas en Teun.

REFERENCES

Barratt, D. C., Davies, A. H., Hughes, A. D., Thom, S. A., & Humphries, K. N. (2001). Optimisation and evaluation of an electromagnetic tracking device for high-accuracy three-dimensional ultrasound imaging of the carotid arteries. *Ultrasound in Medicine and Biology*, *27*(7), 957–968. https://doi.org/10.1016/S0301-5629(01)00395-7

Blackall, J. M., Rueckert, D., Maurer, C. R., Penney, G. P., Hill, D. L. G., & Hawkes, D. J. (2000). An image registration approach to automated calibration for freehand 3D ultrasound. *Lecture Notes in Computer Science (Including Subseries Lecture Notes in Artificial Intelligence and Lecture Notes in Bioinformatics)*, *1935*, 462–471. https://doi.org/10.1007/978-3-540-40899-4_47

Cai, Q., Peng, C., Prieto, J. C., Rosenbaum, A. J., Stringer, J. S. A., & Jiang, X. (2019). A Low-Cost Camera-Based Ultrasound Probe Tracking System: Design and Prototype. *2019 IEEE International Ultrasonics Symposium (IUS)*, 997–999. https://doi.org/10.1109/ULTSYM.2019.8925631

Carbajal, G., Lasso, A., Gómez, A., & Fichtinger, G. (2013). Improving N-wire phantom-based freehand ultrasound calibration. *International Journal of Computer Assisted Radiology and Surgery*, *8*(6), 1063–1072. https://doi.org/10.1007/s11548-013-0904-9

Chan, V. S., Mohamed, F., Yusoff, Y. A., Dewi, D. E. O., Anuar, A., Shamsudin, M. A., & Mong, W. S. (2020). Using game controller as position tracking sensor for 3D freehand ultrasound imaging. *Medical and Biological Engineering and Computing*, *58*(5), 889–902. https://doi.org/10.1007/s11517-019-02044-4

Chen, T. K., Thurston, A. D., Ellis, R. E., & Abolmaesumi, P. (2009). A Real-Time Freehand Ultrasound Calibration System with Automatic Accuracy Feedback and Control. *Ultrasound in Medicine and Biology*, *35*(1), 79–93. https://doi.org/10.1016/j.ultrasmedbio.2008.07.004

Doi, M., Matsusaka, K., Oshiro, O., & Chihara, K. (1999). 3D echocardiography synchronized with cardiac cycle. *Proceedings of the First Joint BMES/EMBS Conference. 1999 IEEE Engineering in Medicine and Biology 21st Annual Conference and the 1999 Annual Fall Meeting of the Biomedical Engineering Society (Cat. N*, *2*, 1060 vols.2-. https://doi.org/10.1109/IEMBS.1999.804217

Fedorov, A., Beichel, R., Kalpathy-Cramer, J., Finet, J., Fillion-Robin, J. C., Pujol, S., Bauer, C., Jennings, D., Fennessy, F., Sonka, M., Buatti, J., Aylward, S., Miller, J. V., Pieper, S., & Kikinis, R. (2012). 3D Slicer as an image computing platform for the Quantitative Imaging Network. *Magnetic Resonance Imaging*. https://doi.org/10.1016/j.mri.2012.05.001

Fenster, A., Blake, C., & Downey, D. B. (1999). Three-dimensional ultrasound-guided minimally invasive therapy of the prostate. *IMTC/99. Proceedings of the 16th IEEE Instrumentation and Measurement Technology Conference (Cat. No.99CH36309)*, *1*, 350–353 vol.1. https://doi.org/10.1109/IMTC.1999.776774

Fenster, A., Downey, D. B., & Cardinal, H. N. (2001). Three-dimensional ultrasound imaging. *Physics in Medicine and Biology*, *46*(5), R67-99. https://doi.org/10.1088/0031-9155/46/5/201

Franz, A. M., Haidegger, T., Birkfellner, W., Cleary, K., Peters, T. M., & Maier-Hein, L. (2014). Electromagnetic tracking in medicine -A review of technology, validation, and applications. *IEEE Transactions on Medical Imaging*. https://doi.org/10.1109/TMI.2014.2321777

Gao, H., Huang, Q., Xu, X., & Li, X. (2016). Wireless and sensorless 3D ultrasound imaging. *Neurocomputing*, *195*, 159–171. https://doi.org/10.1016/j.neucom.2015.08.109

Goldsmith, A. M., Pedersen, P. C., & Szabo, T. L. (2008). An inertial-optical tracking system for portable, quantitative, 3D ultrasound. *2008 IEEE Ultrasonics Symposium*, 45–49. https://doi.org/10.1109/ULTSYM.2008.0012

Herickhoff, C. D., Morgan, M. R., Broder, J. S., & Dahl, J. J. (2018a). Low-cost Volumetric Ultrasound by Augmentation of 2D Systems: Design and Prototype. *Ultrasonic Imaging*, *40*(1), 35–48. https://doi.org/10.1177/0161734617718528

Herickhoff, C. D., Morgan, M. R., Broder, J. S., & Dahl, J. J. (2018b). Low-cost Volumetric Ultrasound by Augmentation of 2D Systems: Design and Prototype. *Ultrasonic Imaging*, *40*(1), 35–48. https://doi.org/10.1177/0161734617718528

Housden, R James, Gee, A. H., Treece, G. M., & Prager, R. W. (2007). Sensorless reconstruction of unconstrained freehand 3D ultrasound data. *Ultrasound in Medicine & Biology*, *33*(3), 408–419. https://doi.org/10.1016/j.ultrasmedbio.2006.09.015

Housden, Richard James, Treece, G. M., Gee, A. H., & Prager, R. W. (2008). Calibration of an orientation sensor for freehand 3D ultrasound and its use in a hybrid acquisition system. *BioMedical Engineering Online*, *7*, 1–13. https://doi.org/10.1186/1475-925X-7-5

Huang, Q.-H., Yang, Z., Hu, W., Jin, L.-W., Wei, G., & Li, X. (2013). Linear tracking for 3-D medical ultrasound imaging. *IEEE Transactions on Cybernetics*, *43*(6), 1747–1754. https://doi.org/10.1109/TSMCC.2012.2229270

Huang, Q. H., Zheng, Y. P., Lu, M. H., & Chi, Z. R. (2005). Development of a portable 3D ultrasound imaging system for musculoskeletal tissues. *Ultrasonics*, *43*(3), 153–163. https://doi.org/10.1016/j.ultras.2004.05.003

Huang, Q., Wu, B., Lan, J., & Li, X. (2018). Fully Automatic Three-Dimensional Ultrasound Imaging Based on Conventional B-Scan. *IEEE Transactions on Biomedical Circuits and Systems*, *12*(2), 426–436. https://doi.org/10.1109/TBCAS.2017.2782815

Huang, X., & Wu, X. (2019). An Electromagnetic Tracking Method Based on Phase Difference Detection. *IEEE Transactions on Magnetics*, *55*(9), 1–8. https://doi.org/10.1109/tmag.2019.2915264

Kok, M., Hol, J. D., & Schön, T. B. (2017). Using inertial sensors for position and orientation estimation. In *Foundations and Trends in Signal Processing*. https://doi.org/10.1561/2000000094

Leotta, D. F. (2004). An efficient calibration method for freehand 3-D ultrasound imaging systems. *Ultrasound in Medicine & Biology*, *30*(7), 999–1008. https://doi.org/10.1016/j.ultrasmedbio.2004.05.007

Lindseth, F., Langø, T., Bang, J., & Nagelhus Hernes, T. A. (2002). Accuracy evaluation of a 3D ultrasound-based neuronavigation system. *Computer Aided Surgery : Official Journal of the International Society for Computer Aided Surgery*, *7*(4), 197–222. https://doi.org/10.1002/igs.10046

Lindseth, F., Tangen, G. A., Langø, T., & Bang, J. (2003). Probe calibration for freehand 3-D ultrasound. *Ultrasound in Medicine & Biology*, *29*(11), 1607–1623. https://doi.org/10.1016/s0301-5629(03)01012-3

Mercier, L., Langø, T., Lindseth, F., & Collins, D. L. (2005a). A review of calibration techniques for freehand 3-D ultrasound systems. *Ultrasound in Medicine and Biology*, *31*(4), 449–471. https://doi.org/10.1016/j.ultrasmedbio.2004.11.015

Mercier, L., Langø, T., Lindseth, F., & Collins, D. L. (2005b). A review of calibration techniques for freehand 3-D ultrasound systems. *Ultrasound in Medicine & Biology*, *31*(4), 449–471. https://doi.org/10.1016/j.ultrasmedbio.2004.11.015

Moher, D., Liberati, A., Tetzlaff, J., Altman, D. G., Altman, D., Antes, G., Atkins, D., Barbour, V., Barrowman, N., Berlin, J. A., Clark, J., Clarke, M., Cook, D., D'Amico, R., Deeks, J. J., Devereaux, P. J., Dickersin, K., Egger, M., Ernst, E., … Tugwell, P. (2009). Preferred reporting items for systematic reviews and meta-analyses: The PRISMA statement. In *PLoS Medicine*. https://doi.org/10.1371/journal.pmed.1000097

Mozaffari, M. H., & Lee, W.-S. (2017a). Freehand 3-D Ultrasound Imaging: A Systematic Review. *Ultrasound in Medicine & Biology*, *43*(10), 2099–2124. https://doi.org/10.1016/j.ultrasmedbio.2017.06.009

Mozaffari, M. H., & Lee, W. S. (2017b). Freehand 3-D Ultrasound Imaging: A Systematic Review. *Ultrasound in Medicine and Biology*, *43*(10), 2099–2124. https://doi.org/10.1016/j.ultrasmedbio.2017.06.009

Pagoulatos, N., Rohling, R. N., Edwards, W. S., & Kim, Y. (2000). <title>New spatial localizer based on fiber optics with applications in 3D ultrasound imaging</title>. *Medical Imaging 2000: Image Display and Visualization*, *3976*(April 2000), 595–602. https://doi.org/10.1117/12.383088

Prager, R. W., Rohling, R. N., Gee, A. H., & Berman, L. (1998). Rapid calibration for 3-D freehand ultrasound. *Ultrasound in Medicine and Biology*, *24*(6), 855–869. https://doi.org/10.1016/S0301-5629(98)00044-1

Prager, Richard W, Gee, A., & Berman, L. (1999). Stradx: real-time acquisition and visualization of freehand three-dimensional ultrasound. *Medical Image Analysis*, *3*(2), 129–140. https://doi.org/10.1016/s1361-8415(99)80009-7

Prager, Richard W, Gee, A. H., Treece, G. M., Cash, C. J. C., & Berman, L. H. (2003). Sensorless freehand 3-D ultrasound using regression of the echo intensity. *Ultrasound in Medicine & Biology*, *29*(3), 437–446. https://doi.org/10.1016/s0301-5629(02)00703-2

Prevost, R., Salehi, M., Jagoda, S., Kumar, N., Sprung, J., Ladikos, A., Bauer, R., Zettinig, O., & Wein, W. (2018). 3D freehand ultrasound without external tracking using deep learning. *Medical Image Analysis*, *48*, 187–202. https://doi.org/10.1016/j.media.2018.06.003

Rafii-Tari, H., Abolmaesumi, P., & Rohling, R. (2011). Panorama ultrasound for guiding epidural anesthesia: A feasibility study. *Lecture Notes in Computer Science (Including Subseries Lecture Notes in Artificial Intelligence and Lecture Notes in Bioinformatics)*, *6689 LNCS*, 179–189. https://doi.org/10.1007/978-3-642-21504-9_17

Rahni, A. A. A., & Yahya, I. (2007). Obtaining translation from a 6-DOF MEMS IMU - An overview. *2007 Asia-Pacific Conference on Applied Electromagnetics Proceedings, APACE2007*, 7–11. https://doi.org/10.1109/APACE.2007.4603861

Royston, P. (1992). Approximating the Shapiro-Wilk W-test for non-normality. *Statistics and Computing*. https://doi.org/10.1007/BF01891203

Sadjadi, H., Hashtrudi-Zaad, K., & Fichtinger, G. (2016). Simultaneous localization and calibration for electromagnetic tracking systems. *The International Journal of Medical Robotics + Computer Assisted Surgery : MRCAS*, *12*(2), 189–198. https://doi.org/10.1002/rcs.1670

Schafer, R. W. (2011). *What Is a Savitzky-Golay Filter? [Lecture Notes]*. *July*, 111–117.

Sofka, M., Zhang, J., Good, S., Zhou, S. K., & Comaniciu, D. (2014). Automatic detection and

measurement of structures in fetal head ultrasound volumes using sequential estimation and Integrated Detection Network (IDN). *IEEE Transactions on Medical Imaging*, *33*(5), 1054–1070. https://doi.org/10.1109/TMI.2014.2301936

Strobl, K. H., & Hirzinger, G. (2006). Optimal hand-eye calibration. *IEEE International Conference on Intelligent Robots and Systems*. https://doi.org/10.1109/IROS.2006.282250

Sun, S.-Y., Gilbertson, M., & Anthony, B. W. (2014). Probe localization for freehand 3D ultrasound by tracking skin features. *Medical Image Computing and Computer-Assisted Intervention : MICCAI ... International Conference on Medical Image Computing and Computer-Assisted Intervention*, *17*(Pt 2), 365–372. https://doi.org/10.1007/978-3-319-10470-6_46

Treece, G. M., Gee, A. H., Prager, R. W., Cash, C. J. C., & Berman, L. H. (2003). High-definition freehand 3-D ultrasound. *Ultrasound in Medicine and Biology*, *29*(4), 529–546. https://doi.org/10.1016/S0301-5629(02)00735-4

van den Heuvel, T. L. A. (2019). *Automated low-cost ultrasound: improving antenatal care in resource-limited settings*.

Wohlin, C. (2014). Guidelines for snowballing in systematic literature studies and a replication in software engineering. *ACM International Conference Proceeding Series*. https://doi.org/10.1145/2601248.2601268

APPENDIXES

Appendix 1: Literature review

Overview of the methods for position tracking, calibration and performance assessment in three-dimensional ultrasound imaging: a systematic review

Abstract

Three-dimensional (3D) ultrasound is used in a variety of applications because of its ability to view two-dimensional (2D) cross-sectional images in any orientation and to perform quantitative volume measurements of complex structures. The increasing interests has led to the development of various methods for 3D ultrasound acquisition. This systematic review gives an overview of the methods used for position tracking and calibration to create a 3D ultrasound volume with 2D ultrasound images. Furthermore, this review gives an overview of the performance assessment methods for 3D ultrasound imaging.

A literature search was performed between June and July 2020 in IEEE Xplore and PubMed. A total of 578 references were identified and assessed on relevance by skim reading. This resulted in 45 selected references which were searched with the snowball method and reference searching, resulting in a total of 9 additional references, giving a total of 54 references. After reading the 54 selected references, a total of 25 references have been included in this systematic review, on the condition that the output described a 3D ultrasound acquisition method and gave a performance assessment.

Unfortunately, the overview of the methods for position tracking, calibration and performance assessment does not enable the comparison between different acquisition methods, as the performance depends on more variables. We therefore conclude that new published references should provide a more thorough overview of the variables that affect performance. This review contributes to an unified performance assessment system with an overview and categorization description of the methods for position tracking, calibration and performance assessment in 3D ultrasound volumes formed with 2D ultrasound images.

Introduction

Three-dimensional (3D) ultrasound imaging has been a well-studied topic in the literature over the past decades and it has been used in a variety of applications, including cardiac imaging, transrectal imaging and prenatal screening (Mozaffari & Lee, 2017b). The growing interests are due to the low-cost solution for 3D medical imaging and due to the advantages over conventional two-dimensional (2D) ultrasound imaging (Fenster et al., 2001). In comparison with conventional 2D ultrasound images, a 3D ultrasound volume enable viewing of 2D cross-sectional images in any orientation and quantitative volume measurements of complex structures (Sofka et al., 2014).

To be able to acquire a 3D ultrasound volume we define the following three steps: step one, 2D ultrasound image (B-scan) acquisition with the corresponding positional information; step two, pre-processing of the acquired B-scans to increase their quality; and step three, reconstruction of the 3D volume using the positional information to translate the image pixels into the voxels of a 3D volume grid. The objective of this systematic review is to give an overview of methods for position tracking, calibration and performance assessment in 3D ultrasound imaging, whereby the 3D ultrasound volume is formed with 2D ultrasound images. Previous systematic reviews have described the various 3D ultrasound imaging methods and their calibration techniques (Treece et al., 2003; Mercier et al., 2005; Fenster et al., 2001; Franz et al., 2014; Mozaffari & Lee, 2017). This review includes the latest developments in the field of 3D ultrasound imaging and includes an overview of the performance assessment methods. The four main questions addressed in this review are:

1. What are the current methods used for position tracking in 3D ultrasound imaging?
2. Which calibration methods are used in 3D ultrasound imaging?
3. Which performance assessment is used to assess a 3D ultrasound imaging system?
4. How can different 3D ultrasound acquisition methods be compared?

Methods

This systematic review follows the guideline of the Preferred Reporting Items for Systematic Reviews and Meta-analysis (PRISMA) statement, including the checklist and the flow diagram (Moher et al., 2009). A systematic electronic literature search was performed between June 2020 and July 2020 using the databases PubMed and IEEE Xplore, since these databases cover most relevant references in the field of biomedical engineering. The search was supplemented by handsearching, the snowball method and citation searching (Wohlin, 2014). The selection and inclusion of references was performed in four sequential steps, these are: step one, identification of relevant references by searching databases; step two, screening of the references using an article inclusion statement; step three, assessment on eligibility of the screened references and additional literature searching; and step four, listing the included references. The result of each step is shown in Figure 1, which is a modified version of the PRISMA flow diagram (Moher et al., 2009).

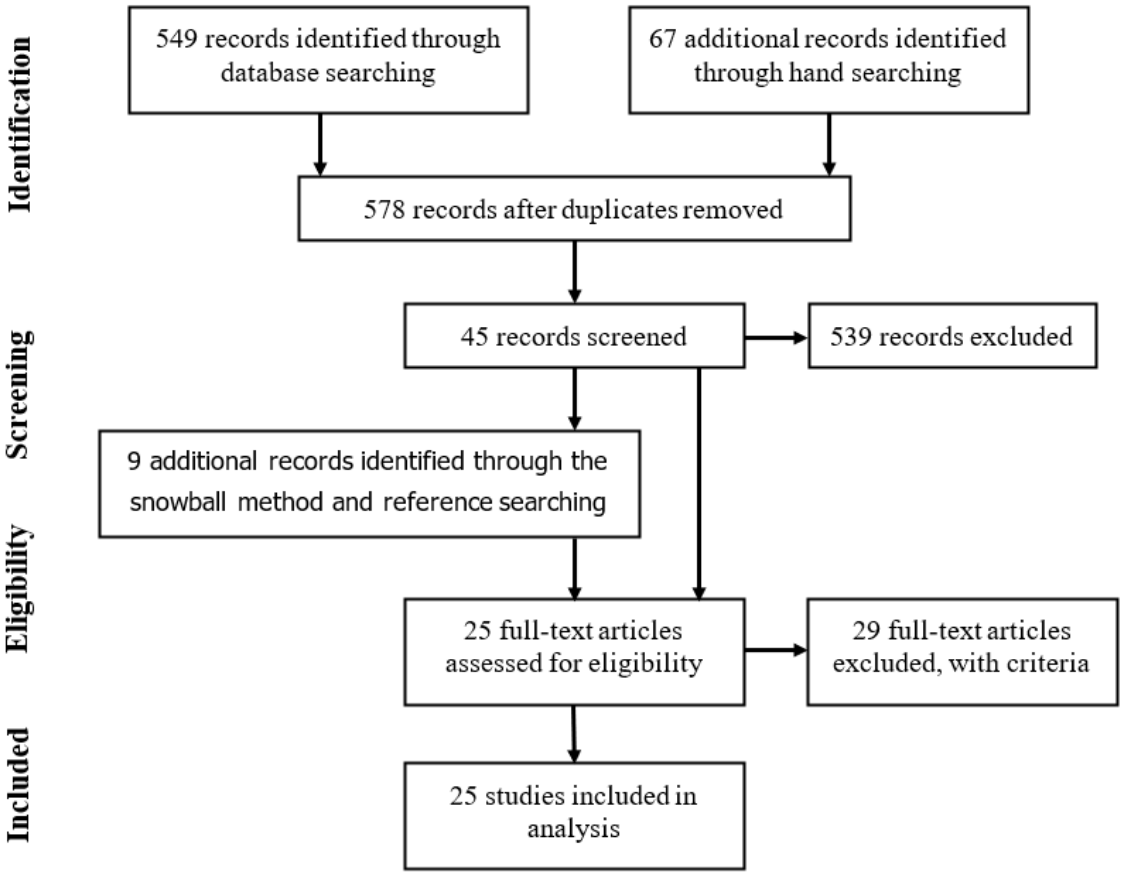

Figure 1. Modified PRISMA flow diagram.

1. Identification

The databases IEEE Xplore and PubMed were searched for relevant references using a search term made out of multiple search blocks connected by operators. Each search block had a different focus and all relevant synonyms were used to include different writing styles. Figure 2 shows a graphical representation of the search blocks with the keywords. Only references published after 1970 were

included in this review, because the first 3D ultrasound references were published in that year (Mozaffari & Lee, 2017b). A total of 549 references were retrieved from the initial search of the databases and handsearching yielded in 67 references. Removing the duplicates with Mendeley Desktop led to a total of 578 references.

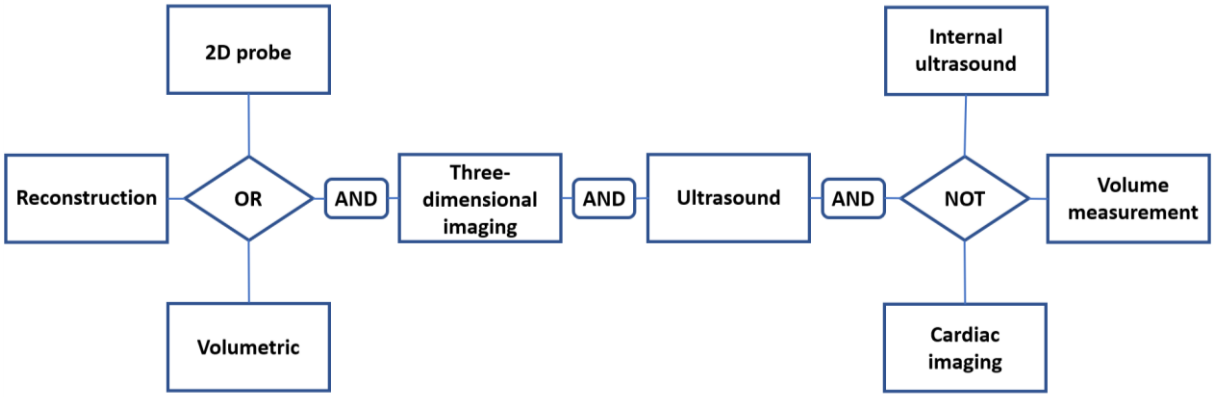

Figure 2. The used search blocks and keywords in the literature search.

2. *Screening*

The total of 578 retrieved references was skim read and assessed using the article inclusion statement. The article inclusion statement is a description of requirements to assess references as relevant. In line with the objective, the output in the selected references must describe a 3D ultrasound acquisition method with a performance assessment. As described in the introduction, we defined 3D ultrasound acquisition as the process from obtaining a 2D ultrasound image until the reconstruction into a 3D image. This review has a focus on step one of 3D ultrasound acquisition: the acquisition of 2D ultrasound images with corresponding positional information. The second step in 3D ultrasound acquisition is the pre-processing of acquired B-scans and the third step is the reconstruction of the 3D volume. Within this review we excluded references that only look at image enhance procedures, e.g. optimal ultrasound settings, or 3D volume reconstruction, e.g. empty voxel filling by interpolation, since these methods can be applied to all acquisition methods.
References describing a clinical application of 3D ultrasound imaging and references describing cardiac or internal ultrasound measurements were also excluded, because of the specific challenges in those applications, e.g. rapid movement or a limit manoeuvrability (Doi et al., 1999; Fenster et al., 1999).
The identified references were assessed by skim reading the title and abstract. A total of 45 references were screened and 539 references were excluded. The 45 screened references were searched with the snowball method and reference searching, resulting in a total of 9 additional references, giving a total of 54 screened references.

3. *Eligibility*

The 54 screened references were assessed for eligibility by full text reading and assessment with the article inclusion statement. A total 29 references were excluded because one or more of the following reasons: they didn't perform an performance assessment; they repeated only repeated the methods described in another reference; the reference output is a 3D ultrasound reconstruction, visualization or volume measurement method. A total of 25 references were included during the assessment by full text reading.

4. *Included*

A total of 25 references have been included (Barratt et al., 2001)(Barratt et al., 2001; Blackall et al., 2000; Cai et al., 2019; V. S. Chan et al., 2020; Gao et al., 2016; Goldsmith et al., 2008; Herickhoff et al., 2018; R James Housden et al., 2007; Richard James Housden et al., 2008; Q.-H. Huang et al., 2013;

Q. Huang et al., 2018; Q. H. Huang et al., 2005; X. Huang & Wu, 2019; Leotta, 2004; Lindseth et al., 2003; Pagoulatos et al., 2000; R. W. Prager et al., 1998; Richard W Prager et al., 1999, 2003; Prevost et al., 2018; Rafii-Tari et al., 2011; Rahni & Yahya, 2007; Sadjadi et al., 2016; Sun et al., 2014; Treece et al., 2003).

Results

The results give an overview of the used 3D ultrasound volume acquisition methods in the included references. The first section covers the position tracking systems. The second section gives an overview of the calibration methods to transform the coordinates of the tracking device into the coordinates of the 3D ultrasound volume. The third section gives an overview of the performance assessment measurements. Table 1 gives an overview of the used methods in the references.

1. Position tracking methods

To form a 3D ultrasound volume, the obtained B-scans are positioned according to their corresponding position and orientation. Therefore, the position and orientation of each image must be tracked during the procedure of the B-scans acquisition. The position tracking systems can be divided into six categories: a 3D ultrasound probe, a 2D scanner with an external fixture, freehand scanning with electromagnetic tracking, freehand scanning with optical tracking, freehand scanning with inertial sensors and freehand sensorless imaging. This review has a focus on methods that form a 3D ultrasound volume using 2D ultrasound images, hence there were no included references describing a 3D ultrasound probe.

1.1. External fixture

With an external fixture the probe is fixed to a mechanical or electromechanical device. The user can move the probe in a haptic manner or create a pre-programmed desired path. The position and orientation of the probe can be precisely determined by the angles formed in each joint of the fixture. This method enables accurate position tracking and precise repeating of the scanning procedure (Chan et al., 2020). On the other hand, an external fixture gives less probe manoeuvrability (Q.-H. Huang et al., 2013). The recent literature about external fixture position tracking is focussed on automated systems and the manoeuvrability of the probe.
In 2013 Huang *et al.* developed a linear tracking system for 3D ultrasound imaging (Q.-H. Huang et al., 2013). A fixture allowed movements with one degree of freedom, giving the system at the same time a good performance and manoeuvrability in that direction. In 2018 another group, Huang *et al.,* developed a fully automated and user independent 3D ultrasound imaging system (Q. Huang et al., 2018). The probe was fixed to a 3D translating device to move the probe on the tissue surface. The probe trajectory was automatically planned with a camera measuring the depth. In addition, two force sensors were used to maintain an equal pressure on the tissue. This fully automated 3D ultrasound imaging system has a good performance due to the mechanical fixture and a good manoeuvrability of the probe due to the 3D translation device.

1.2. Electromagnetic tracking

In freehand scanning with electromagnetic tracking the position of the ultrasound probe can be determined by using a magnetic field, generated by either an alternating current or direct current transmitter, and magnetic sensors mounted on the ultrasound probe. The most common method to determine the position and orientation is with a magnetic field of at least three field generators and with two sensors mounted on the probe, giving a six degree of freedom system. If only one sensor is used, the system becomes a system with five degrees of freedom, because a coil is axially symmetrical. The relative strengths of the induced currents in the sensors when sequentially activating the field generators enable the calculation of the position and orientation of the sensor (Barratt et al., 2001). Although this position reconstruction method is common, the solution is restricted to the disadvantages of iterative problem solving. An iterative solution can result in

disadvantages such as converge to a local extreme point of fail to converge if an inappropriate initial point is chosen (X. Huang & Wu, 2019). Another, recently published method tries to overcome the limitations of iterative methods and introduces position tracking based on phase difference detection (X. Huang & Wu, 2019). Using three field generators and three magnetic sensors, the position and orientation of the sensors can be obtained by measuring the phase difference between the excitation current of the field generator and the induction current of the sensor.
The main advantages of electromagnetic tracking systems are the non-restricted manoeuvrability of the probe and the signal passing through the body. The main disadvantage is the system's sensitivity to metallic objects placed too close to the field generator or magnetic sensor, due to ferromagnetism and eddy currents (Barratt et al., 2001; Sadjadi et al., 2016). Another source of distortion is the distance and orientation between the field generator and the magnetic sensor do affect the quality of the measurements. Each generator-sensor combination has a separation at which the best measurements can be obtained (Barratt et al., 2001).

1.3. Optical tracking

An optical tracking method is defined as a method that uses a camera to track to the position of the probe. The most common method is indirect position tracking whereby at least three markers and one camera are required to track the position and orientation of the probe with six degrees of freedom, addition markers increase the probe visibility and performance. The markers are mounted on the probe and can be active, light-emitting, or passive, light reflecting (Cai et al., 2019; Lindseth et al., 2003; Treece et al., 2003). To improve the portability and decrease the costs of the system, an optical tracking solution is proposed by Goldsmith *et al*. whereby the probe position is localized by a camera looking at skin features (Goldsmith et al., 2008; Sun et al., 2014). A camera mounted on the probe looks at skin features and compares this with a skin map to determine the probe position.
Another camera based position tracking method uses a camera mounted on the probe and a specialized adhesive marker strip attached to the skin (Pagoulatos et al., 2000; Rafii-Tari et al., 2011). The position of the probe is determined by the camera looking at and identifying the markers on the strip.
Among the freehand techniques, optical tracking has the best performance (Treece et al., 2003). However, this performance is dependent on the position and orientation of the markers to the camera, the system requires a line of sight between the camera and the markers.

1.4. Inertial sensors

When using inertial sensors for freehand position tracking the orientation and position of the probe are determined by an accelerometer and a gyroscope. The combination of the output of these sensors enables the calculation of the position of the probe (Chan et al., 2020; Herickhoff et al., 2018b). However, this kind of position determination is highly sensible for drift errors, mainly because the accelerometer data is twice integrated (Herickhoff et al., 2018b; Rahni & Yahya, 2007). Therefore, the inertial sensors themselves are often used as orientation measurement device, without position determination. The orientation determination of inertial sensors have a good performance and can be used in combination with another tracking method to track the probe position with six degrees of freedom (Chan et al., 2020; Goldsmith et al., 2008; R James Housden et al., 2007).
Herickhoff *et al.* describes a system for 3D ultrasound imaging combining the inertial sensors. The drift problem is solved with an external fixture to stabilize and restrict the probe motion to pivoting at a single position, see Figure 3. Other groups have described the use of inertial sensors as orientation device in combination with another tracking method used for position determination. Chan *et al.* used optical tracking for the position determination, Goldsmith and Szabo created a system whereby the position is optically tracked looking at skin features with a camera mounted on the probe and Housden *et al.* combined inertial sensors with sensorless imaging (Chan et al., 2020; Goldsmith et al., 2008; R James Housden et al., 2007).

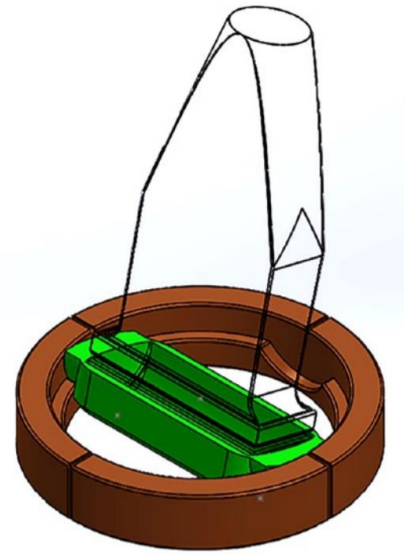

Figure 3. *Probe fixture for one-degree of freedom imaging with inertial sensors* (Herickhoff et al., 2018b).

1.5. Sensorless imaging

In sensorless imaging the position and orientation of the probe are determined without an external position tracking device, using only the 2D ultrasound images themselves. The goal in sensorless imaging methods is to find the local transformation between successive pairs of 2D ultrasound images. The problem of local transformation of in-plane motion, a translation along the ultrasound plane, is solved by registration solutions. These registration solutions align corresponding features of neighbouring images. The problem of out-of-plane motion, elevational direction, is solved using speckle decorrelation. The speckle patterns of successive pairs of 2D ultrasound images are correlated, because ultrasound image intensities undergo a point-spread function not only in the image plane but also in the perpendicular direction. The correlation gives information about the out-of-plane movement: the higher the correlation, the lower the elevational movement and vice versa, see Figure 4 (R James Housden et al., 2007; Richard W Prager et al., 2003). Another sensorless method make use of a deep learning algorithm to determine the movement between successive 2D ultrasound images (Prevost et al., 2018). The system is trained with ultrasound sweeps of the forearms and lower legs whereby the convolutional neural network must match the ground truth, determined by optical tracking. A 3D ultrasound volume is reconstructed based on the determined translational and elevational motion between successive 2D ultrasound images.
Although sensorless imaging has a great potential due to its portability and low costs, the method cannot reach the performance of other freehand tracking methods (Richard James Housden et al., 2008). The main performance limitation is caused by large scale drift as a result of small biases in the speckle correlation. The speckle correlation assumes solely elevational motion, so rotational motion results in a systematic overestimation (R James Housden et al., 2007).

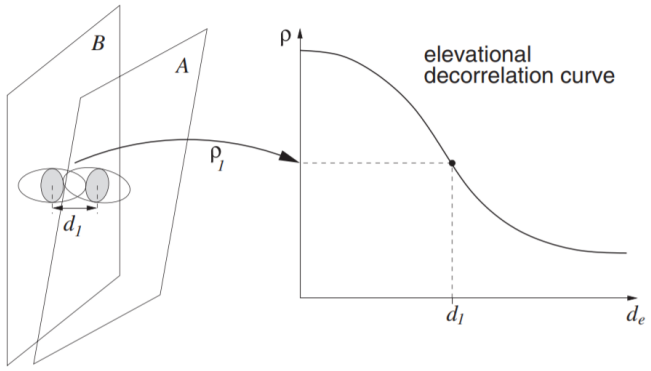

Figure 4. The elevational decorrelation curve shows the relationship with the speckle correlation and the distance between successive images (R James Housden et al., 2007).

2. Calibration methods

A calibration step is required to correctly place the acquired 2D ultrasound images into the 3D ultrasound volume. During calibration the transformation between the coordinates of the position tracking method and the coordinates of the acquired ultrasound image is determined. Calibrations are required for position tracking methods whereby the coordinates of the position tracking are not the same as the 2D ultrasound image, therefore sensorless methods do not require calibration.

Calibration can be divided into temporal and spatial calibration. Temporal calibration is necessary to determine the offset between the position sensor time-stamps and the B-scan time-stamps. Spatial calibration determines the transformation between the position and orientation of the coordinate system of the B-scan and the coordinate system of the tracking device (R. W. Prager et al., 1998). Spatial calibration is based on the match of the positional information and the B-scan acquisition at a specific time-stamp, this match is determined in the temporal calibration. Hence, temporal calibration is performed first. Below the various temporal and special calibrations are described, Table 1 gives an overview of the used methods in the included references.

2.1. Temporal calibration

The goal of temporal calibration is to match the time-stamps of the acquired B-scans with the positional data. This calibration step is performed before spatial calibration and must therefore be designed without knowledge of the location or size of the B-scan. The temporal calibration method is subdivided into three methods.

2.1.1. Step input

The temporal calibration of Prager *et al.* is based on sudden changes in the B-scan and position readings (Richard W Prager et al., 1999). By holding the probe still and suddenly jerking it away, the discrepancy in the timing between the tracking device and the B-scan can be measured. This latency between the two data streams give an offset to adjust the tracking device time-stamps.

2.1.2. Cross-correlation

Treece et al. developed a method based on the cross-correlation between the depth derived from the B-scan and the positional information from the tracking device while moving the probe up and down in a bath full of water (Treece et al., 2003). Before cross-correlation, the depths derived from the B-scans and the position data of the tracking devices were both normalized. The temporal offset is found that gives the minimum root-mean-square error between the normalized depth distances derived from the B-scan and those derived from the position sensor.
A disadvantage of the method developed by Treece *et al.* is the assumption of solely vertical movement during the procedure. Without spatial calibration the direction of the probe movement can't be determined. Treece *et al.* assumes perfect vertical movement, so horizontal movement

leads to errors in the temporal calibration. Huang *et al.* solved this problem by using a 3D translation device to control the movement of the probe in steady vertical movement (Q. H. Huang et al., 2005). Another improvements to the method of Treece *et al.* is the use of a bone instead of a bath full of water, this enables in-vivo temporal calibration (Prevost et al., 2018).

2.1.3. Time marks

Huang *et al.* developed a different method for temporal calibration which was performed after spatial calibration (Q.-H. Huang et al., 2013). In their method a stick with eight fixed silicon balls was scanned. When the B-scan showed the centre of a silicon ball the time was marked. The time marks were used to obtain the position measured by the position sensor at that specific time. Both positions, recorded at the same time-mark, were normalized according to the range between the balls. The time offset was found that gives the minimum root-mean-square between the cross-correlation of the normalized distances.

2.2. Spatial calibration

The goal of spatial calibration is to transform the coordinates of the positional data of the tracking device mounted to the probe to the coordinates of the B-scans. The most straightforward method to determine the translational parameters is to perform external measurements of the probe casting and its attached sensor (Lindseth et al., 2003). However, the origin of the B-scan and of the magnetic sensors is hard to determine. In addition, this calibration method does not take the rotational parameters into account. A common approach to overcome these limitations is to scan a phantom with known geometric properties. This phantom must be scanned across all degrees of freedom to obtain valid calibration parameters. The spatial calibrations based on phantom imaging are divided over multiple categories. Besides phantom based calibration, another category is non-phantom based calibration methods.

2.2.1. Non-phantom calibration

In the non-phantom calibration methods the signal of the system is correlated with the movement of the probe. Pagoulatos *et al.* developed an optical tacking method based on a strip with optical markers (Pagoulatos et al., 2000). To determine the orientation while scanning along the strip a calibration step was performed. In this calibration step, special markers are used that got a direct proportionality between the light output and the amount of bending. The calibration correlated the light output of the markers with the orientation of the camera.
Goa *et al.* developed a sensorless imaging method (Gao et al., 2016). In the calibration step the speckle correlation between two images with a known distance is determined. The result of this calibration is a decorrelation curve to compute the distance between two images based on the speckle correlation, see Figure 4.
Herickhoff *et al.* developed a single degree of freedom 3D ultrasound system, whereby the calibration step involved placing the probe steady on the patient's sternum and saving the orientation as reference measurement (Herickhoff et al., 2018b).
Sadjadi *et al.* refers to a calibration technique described by Strobl and Hirzinger called hand-eye nonlinear optimization, a thorough explanation can be found in (Strobl & Hirzinger, 2006) (Sadjadi et al., 2016). Furthermore, they describe dynamic calibration of tracking devices, whereby the spatial calibration is constantly updated. The main advantage of this method is that the calibration is also valid in a changing environment, for example with magnetic field distortions. The model of Sadjadi *et al.* uses a predefined trajectory and three redundant electromagnetic sensors to update pre-calibrated parameters in real-time with statistical analyses.

2.2.2. Phantom-based methods

The phantom-based methods are subcategorized into point-based methods, distance-based methods, 2D alignment methods, freehand methods, three-wire phantoms and multimodal calibration.

2.2.2.1. Point-based methods

Characteristic for the point-based methods is to image a point target from several directions to exceed the problem's degree of freedom. In each viewing angle the position of the point target is segmented on the image and the offset with the positional data of the tracking device is used for calibration. In the literature three phantoms have been found which can be used in the point-based calibration method. The first phantom is a small spherical object such as a bead or a pin head. The performance of this method is depended on how well the centre of the point can be located in the phantom and on the image (R. W. Prager et al., 1998). The second phantom is a wire-cross, whereby it is easier to determine the centre of the point. The location where the wires cross is scanned repeatedly from different direction and the wires help to determine the centre of the point (R. W. Prager et al., 1998). The third point-based phantom is the Cambridge phantom developed by Prager *et al.* (R. W. Prager et al., 1998). In the Cambridge phantom a line is produced on the ultrasound image by fixing a bar in the centre of the ultrasound beam. The bar is attached to a setup whereby all degrees of freedom can be images while keeping the bar in the centre of the ultrasound beam, the setup is shown in Figure 5. The Cambridge method is the fasted point-based method, because the bar is easy to detect in the image (R. W. Prager et al., 1998). A disadvantage of this method is the requirement to repeat the spatial calibration whenever the relative locations or size change between the position sensor and the ultrasound probe and the B-scan. Pan, zoom and depth changes require a new set of spatial calibration parameters (Treece et al., 2003).

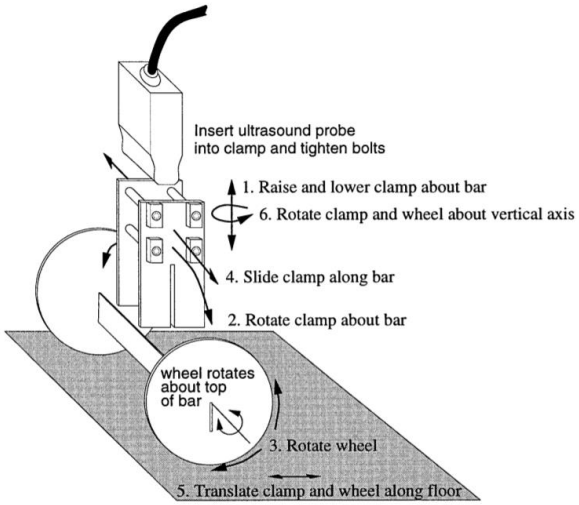

Figure 5. The Cambridge phantom (R. W. Prager et al., 1998).

2.2.2.2. 2D alignment methods

In the 2D alignment methods a phantom with a planar set of points-of-interest is aligned with the ultrasound image. The orientation of the ultrasound image with respect to the phantom is unambiguous, therefore just one image is needed for calibration. However, the ultrasound plane has a finite thickness causing difficulties with aligning out-of-plane phantom features and using just one image results in a poor accuracy (Lindseth et al., 2003). Hence, often several images are taken to improve the quality of the calibration. The 2D alignment method can be used in multiple ways. Huang *et al.* developed a phantom on a flat table with 25 small silicon balls aligned in 5 rows and 5 sets, whereby the balls of each set had a different hight (Q.-H. Huang et al., 2013). The calibration

gives a translation matrix between the location of the balls in the ultrasound image and the measured location of the balls. Another 2D alignment method was described by Leotta (Leotta, 2004). The method is based on the alignment of an ultrasound image plane with a planar array of strings with beads. The calibration parameters are calculated by matching the exact position of three strings and one bead in the image and phantom. Additional out-of-plane coplanar strings help in the alignment process to improve the performance of the calibration method.

2.2.2.3. Freehand methods

Freehand calibration enables calibration of an ultrasound tracking device in a freehand manner. Whereas in the other methods the geometric differences between the phantom and the ultrasound image must be measured, here the position and orientation offset of the probe can be determined based on the unique distribution of points appearing in the ultrasound images. Only one image is needed for the calibration, however in practice it is easy to obtain several and thereby increase performance (Lindseth et al., 2003).

The phantoms used in freehand methods are commonly called Z-fiducial or N-fiducial phantoms. These phantoms contain wires in a Z-shape, creating two similar triangles with known geometry, which are intersected by the image plane, as illustrated in Figure 6 of (Lindseth et al., 2003). With similar shaped triangles and goniometry it is possible to compute the coordinates of the wire crossings in the image. These wire crossings are compared with the known geometry for the systems calibration (Lindseth et al., 2003).

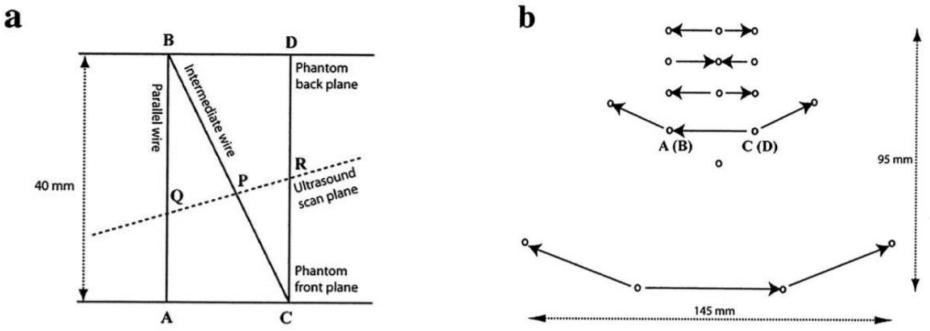

Figure 6. Z-fiducial phantom used by (Lindseth et al., 2003). (a) Top view of the phantom showing one Z structure that consists of three wires. (b) Frond view of the phantom showing a total of 12 Z structures.

2.2.2.4. Three-wire phantom

The three-wire phantom got similarities with the point-based and freehand methods (R. W. Prager et al., 1998). Three wires are mounted in orthogonal directions and scanned along each wire. To determine the calibration parameters it must be known which wire is scanned, which enables the determination of the relative position and orientation. This method has the simplicity of a single point and the flexibility of a freehand method. The performance depends on the orthogonality and straightness of the wires.

2.2.2.5. Multimodal calibration

A multimodal calibration method was described by Blackall *et al.,* were they compared the ultrasound image with the magnetic resonance imaging (MRI) image of a phantom (Blackall et al., 2000). The calibration parameters were determined by alignment of the 2D ultrasound images to the corresponding plane in the MRI volume. The chosen calibration parameters were those that maximized the similarity between the ultrasound images and the MRI scan. The method requires no feature extraction and is fully automatic.

3. Performance assessment measurements

Multiple questions may be raised to assess the performance of a 3D ultrasound acquisition system. Prager *et al.* assessed the performance by answering the three questions "If I do another calibration tomorrow, will I get the same result?", "Given a calibration, if I look at a point from different angles, will it always map to precisely the same point in the reconstruction volume?" and "If I scan something that is 100 mm long in the real world, will come out as 100 mm long in the reconstruction?" (R. W. Prager et al., 1998). Treece *et al.* asked different questions to compare their system performance with other systems: "What part is included in the measurements", "What is it a measurement of?" and "How are the measurements analysed?"(Treece et al., 2003). The answers to these questions can be categorized into the basic quality measures precision and accuracy. Precision is the deviation of multiple measurements of the same object and can be subcategorized into measurement variation, calibration reproducibility and reconstruction precision. Accuracy is the comparison of measurements with the best independent measurement available and can be subcategorized into point-based measures, distance-based measures, volume error, surface error and statistical analysis. The quality measures are explained below and the used measures in the references can be found in Table 1.

3.1. Precision

Precision is a measure of the repeatability of a measurement. A good precision result does not mean a correct result, because the precision does not test the validity of the measurement (Leotta, 2004). The used precision measurements in the included references can be categorized into three categories: measurement variation, calibration reproducibility and reconstruction precision.

3.1.1. Measurement variation

The first precision measurement is a comparison between the results of different transformation matrices (Treece et al., 2003). The result shows the measurement variation in the spatial calibration parameters or in a single point or distance measurement. The measurement variation is often given as the mean, root-mean-square variation or 95% confidence limit of multiple measurements. This measure answers the question: "What is the measurement variation in the spatial calibration parameter values or in the position or distance measurement?". A low variation between different transformation matrices indicates a good and trustworthy reproducibility of the precision measurement.

3.1.2. Calibration reproducibility

Another precision measure is the calibration reproducibility (Lindseth et al., 2003; R. W. Prager et al., 1998). The reproducibility of calibrations gives answer to the question of Prager: "If I do another measurement, will I get the same result?" (R. W. Prager et al., 1998). The calibration reproducibility looks at the position of a point in the ultrasound image with two different calibration transformation matrices:

$$\Delta CR = \left\| T_{cal,1} x_{tp} - T_{cal,2} x_{tp} \right\|, \quad (1)$$

where ΔCR is the reproducibility measure; x_{tp} is the transformation point of the ultrasound image; and $T_{cal,1}$, $T_{cal,2}$ are the two calibration transformation matrices. As transformation point, Lindseth *et al.* and Blackall *et al.* took the right corner furthest from the transducer and Treece took the four corners points plus the centre of the image and Leotta used points specified every 2 cm in depth along the center and the edges of the of the image up to 16 cm (Blackall et al., 2000; Leotta, 2004; Lindseth et al., 2003; Treece et al., 2003). An outcome of this measure around zero, when using different calibration transformations matrices, corresponds to a good calibration procedure.

3.1.3. Reconstruction precision

Reconstruction precision gives answer to the question of Prager: "If I look at a point from a different angle, will it always map to precisely the same point in the reconstruction volume?" (R. W. Prager et

al., 1998). This measure includes the validity of the calibration matrix by using the calibration matrices to reconstruct targets in independent imaging tests. The method involves point-based imaging from multiple viewing angles and determines the difference in the reconstructed location of the point target:

$$\Delta RP = \left\| T_{rw,view1} T_{cal} x_{view1} - T_{rw,view2} T_{cal} x_{view2} \right\|, \quad (2)$$

where ΔRP is the reconstruction precision measure; $T_{rw,viewi}$ is the transformation from the tracking coordinates to the real world coordinates corresponding to the i^{th} view of the target point; x_{viewi} is the i^{th} target point in the 2D ultrasound image coordinates; and T_{cal} is the calibration transformation matrix (Blackall et al., 2000; Leotta, 2004; R. W. Prager et al., 1998).

3.2. Accuracy

With an accuracy measurement you determine if the point is reconstructed in the right place by comparing reconstructed data with a golden standard. The golden standard is the same measurement done with the best available method, e.g. optical tracking or physical measurements with a calliper (Blackall et al., 2000; Leotta, 2004). The methods found in the included references are categorized into: point-based measures, distance-based measures, volume error, surface error and statistical analysis. Two other shorty mentioned accuracy measures are 3D navigation accuracy and 3D registration accuracy, for an explanation of these two measures the reader is referred to (Lindseth et al., 2003).

3.2.1. Point-based measures

In the point-based measures a reconstructed point is compared with the same point measured with a golden standard (Blackall et al., 2000; Lindseth et al., 2003; Treece et al., 2003). The method indicates the accuracy by which a point can be reconstructed to the correct position. This can be done with data of a 3D reconstruction volume or a 2D image, whereby a 3D point-based accuracy measure refers to measurements applied to the 3D reconstructed volume instead of the 2D image. In 3D as well in 2D, the reconstructed location of a point is compared with the golden standard location:

$$\Delta PBA = \left\| T_{rw,view1} T_{cal} x_{view1} - x_{gs} \right\|, \quad (3)$$

where ΔPBA is the point-based accuracy measure; $T_{rw,viewi}$ is the transformation from the tracking coordinates to the real world coordinates corresponding to the i^{th} view of the target point; x_{viewi} is the i^{th} target point in the ultrasound image coordinates; T_{cal} is the calibration transformation matrix on test; and x_{gs} is the golden standard position.

Lindseth *et al.* considers the point-based measure the best, because it measures the effect of probe calibration on reconstruction and navigation accuracy (Lindseth et al., 2003). A good result indicates that the calibration parameters are accurate and that the volume is correctly positioned in space.

3.2.2. Distance-based measures

The distance-based method compares a known distance, measured with a golden standard, with the same distance measured in the reconstructed 3D ultrasound volume (Blackall et al., 2000; Leotta, 2004; Lindseth et al., 2003; R. W. Prager et al., 1998). This measure indicates the extent to which distances can be correctly reconstructed and hence answers the question of Prager: “If I scan something that is 100 mm long in the real world, will it come out as 100 mm long in the reconstruction?” (R. W. Prager et al., 1998). The chosen distance is often the largest possible, because these distances are likely to show the largest discrepancies. This measurement can also be used to find anisotropic reconstruction problems by comparing measurement with a different measurement direction (Lindseth et al., 2003). The distance-based measure is calculated with

$$\Delta DBA = \left\| T_{rw,view1} T_{cal} x_{view1} - T_{rw,view2} T_{cal} x_{view2}) \right\| - \left\| (x_{gs,1} - x_{gs,2} \right\|, \quad (4)$$

where ΔDBA is the distance-based accuracy measure; $T_{rw,viewi}$ is the transformation from the tracking coordinates to the real world coordinates corresponding to the i^{th} view of the target point; x_{viewi} is the i^{th} target point in the ultrasound image coordinates; T_{cal} is the calibration transformation matrix on test; and x_{gs} is the golden standard position.

3.2.3. Volume error

In the volume-based method the known volume of an object is compared with the reconstructed volume (Goldsmith et al., 2008; Pagoulatos et al., 2000). The measure is calculated as follows:

$$\Delta V = 100 \times \frac{V_{meas} - V_{gs}}{V_{gs}}, \quad (5)$$

where ΔV is the volume error in percentage; V_{meas} is the measured volume; and V_{gs} is the known volume measured with a golden standard. The disadvantage of this method is that a low volume error measurement result does not mean a good volume reconstruction, because two very different 3D segmentations can have similar volumes (Goldsmith et al., 2008).

3.2.4. Surface error

The surface-based method calculates the root-mean-square value of the distances from the reconstructed surface points to the golden standard surface points (Goldsmith et al., 2008). The surface error is calculated in three steps: first, the two surfaces are aligned using a closed point algorithm; second, the smallest distance between the reconstructed volume surface points and the golden standard is determined and recorded; and third, the root-mean-square value of this collection of distances between the surfaces is calculated.

3.2.5. Statistical analysis

Chan et al. uses a statistical analyses and calculates the correlation, R^2 value and the covariance between two variables, a thorough explanation can be found in (Chan et al., 2020).

Reference	Tracking method	Calibration		Performance assessment	
		Temporal calibration	Spatial calibration	Precision/Accuracy	Golden standard
(Q. Huang et al., 2018)	External fixture	Cross-correlation	2D alignment	Accuracy: distance-based measure	Known phantom dimensions
(Q.-H. Huang et al., 2013)	External fixture	Time marks	2D-alignment	Accuracy: distance-based measure	Known phantom dimensions
(Barratt et al., 2001)	Electromagnetic tracking	-	-	Precision: measurement variation Accuracy: distance-based measure	Physical measurement
(Q. H. Huang et al., 2005)	Electromagnetic tracking	Cross-correlation	Point-based	Precision: measurement variation Accuracy: distance-based measure Volume error	Known phantom dimensions
(X. Huang & Wu, 2019)	Electromagnetic tracking	-	-	Precision: measurement variation Accuracy: point-based measure	-
(Leotta, 2004)	Electromagnetic tracking	-	2D-alingment	Precision: measurement variation Precision: calibration reproducibility Precision: reconstruction Precision Accuracy: distance-based accuracy	Physical measurement
(Lindseth et al., 2003)	Electromagnetic tracking	-	Point-based 2D-alignment Freehand	Precision: calibration reproducibility Accuracy: point-based accuracy Accuracy: distance-based accuracy	Optical
(R. W. Prager et al., 1998)	Electromagnetic tracking	-	Point-based Three-wire	Precision: calibration reproducibility Precision: reconstruction precision Accuracy: reconstruction accuracy	Known phantom dimensions
(Richard W Prager et al., 1999)	Electromagnetic tracking	Step input	Point-based	Qualitative performance assessment*	-
(Sadjadi et al., 2016)	Electromagnetic tracking	Cross-correlation	Hand-eye nonlinear optimization (non-phantom)	Accuracy: distance-based measure	Optical
(Blackall et al., 2000)	Optical tracking	-	Point-based multimodal	Precision: calibration reproducibility Precision: reconstruction Precision Accuracy: point-based measure Accuracy: distance-based measure	Optotrack pointer MRI

(Cai et al., 2019)	Optical tracking	-	-	Precision: measurement variation Accuracy: distance-based measure	Motorized translation and rotation device
(Chan et al., 2020)	Optical tracking	-	-	Accuracy: statistical accuracy analysis	Motorized translation device
(Pagoulatos et al., 2000)	Optical tracking	-	Proportionality calibration (non-phantom)	Accuracy: volume error	Known phantom dimensions
(Rafii-Tari et al., 2011)	Optical tracking	-	Point-based	Accuracy: distance-based measure	Optical
(Sun et al., 2014)	Optical tracking	-	Point-based	Accuracy: distance-based measure	Optical
(Treece et al., 2003)	Optical tracking	Cross-correlation	Point-based	Precision: measurement variation Precision: calibration reproducibility Accuracy: point-based measure Accuracy: distance-based measure	Known phantom dimensions
(Rahni & Yahya, 2007)	Inertial sensors	-	-	Accuracy: distance-based measure	Known phantom dimensions
(Herickhoff et al., 2018b)	Inertial sensors & External fixture	-	Reference measurement (non-phantom)	Qualitative performance assessment*	-
(Goldsmith et al., 2008)	Inertial sensors & Optical tracking	-	-	Accuracy: volume- and surface-based measurement	Known phantom dimensions
(Richard James Housden et al., 2008)	Inertial sensors & sensorless imaging	Cross-correlation	Point-based	Precision: measurement variation Accuracy: distance-based measure	Optical
(Gao et al., 2016)	Sensorless imaging	-	Decorrelation curve (non-phantom)	Accuracy: distance-based measure	Motorized translation device
(R James Housden et al., 2007)	Sensorless imaging	-	-	Accuracy: distance-based measure	Optical
(Richard W Prager et al., 2003)	Sensorless imaging	-	-	Accuracy: distance-based measure	Optical
(Prevost et al., 2018)	Sensorless imaging	-	-	Accuracy: distance-based measure	Optical

*Table 1: Overview of the methods for position tracking, calibration and performance assessment in the included references. *Qualitative performance assessment: performance assessment by an expert on the diagnostic value of the volume reconstruction.*

Discussion

A systematic review was conducted to give an overview of the methods for position tracking, calibration and performance assessment in 3D ultrasound volumes acquisition with 2D ultrasound images. The results show the methods can be categorized and subcategorized, see Table 2. Table 1 shows the position tracking, calibration and performance assessment used in the included references. To compare references, the variables used that affect performance must be the same except the one being tested. With this criteria, only a comparison can be made between (Q. Huang et al., 2018) and (Q.-H. Huang et al., 2013). In addition to the problem of a lack in similarity between methods, there are more variables that affect performance which should be taken into account, these are: the depth settings of the probe (Treece et al., 2003); the type of probe (Lindseth et al., 2003); the probe movement, e.g. linear translation and tilting, during B-scan acquisition (Lindseth et al., 2002); the orientation of the sensor with respect to the receiver (Barratt et al., 2001); digital or analogue 2D ultrasound acquisition (Mercier et al., 2005b); the relative speed of sound in the calibration phantom and in the accuracy measurement (Mercier et al., 2005b; Treece et al., 2003); the iterative solution (Mercier et al., 2005b) and the coupling medium (Mercier et al., 2005b).

Tracking method	**Calibration**		**Performance assessment**	
	Temporal	**Spatial**	**Precision**	**Accuracy**
External fixture	Step input	Non-phantom calibration	Measurement variation	Point-based
Electromagnetic tracking	Cross-correlation	Point-based	Calibration reproducibility	Distance-based
Optical tracking	Time marks	2D alignment	Reconstruction precision	Volume-error
Inertial sensors		Freehand		Surface error
Sensorless imaging		Three-wire		Statistical analysis
		Multimodal		

Table 2. An overview of the methods for Position tracking, calibration and performance assessment in 3D ultrasound imaging.

To be able to determine the performance of a variable, all variables must be the same except for the one variable being tested. Some references have compared the effect of a variable on the performance by changing one variable within an ultrasound setup, Table 3 gives an overview of these references. Mercier tried to compare different references, but had to conclude that it was too difficult to compare them, because of missing information about performance affecting variables (Mercier et al., 2005b). Like in the study of Mercier, the most included references in this review do not provide all the listed variables affecting the performance and could therefore not be used to determine the effect of a variable on the performance. Some included references mention a calibration method shortly, but do not provide enough information to enable a good comparison. Other included articles simply do not provide the essential information about performance affecting variables at all.

Reference	Compared variables
(Barratt et al., 2001)	Two orientations, receiver facing towards and back away the sensor, and three separations,250mm, 500mm and 750mm, between the sensor and receiver
(Blackall et al., 2000)	Two calibration phantoms: multimodal registration and a single cross-wire phantom
(Leotta, 2004)	Two calibration phantoms: single-point and a 2D alignment phantom
(Lindseth et al., 2003)	Three calibration phantoms: single-point, 2D alignment and a freehand phantom Three kinds of probes: flat phased-array, flat linear-array and an intraoperative probe
(R. W. Prager et al., 1998)	Three calibration phantoms: Cambridge, three-wire and single cross-wire
(Prevost et al., 2018)	Four reconstruction methods: linear motion, speckle decorrelation, standard convolutional neural network (CNN) and a CNN with optical flow
(Q.-H. Huang et al., 2013)	Two reconstruction methods: one degree of freedom external fixture and optical tracking
(Treece et al., 2003)	Three probe frequencies and depth settings: 5-10 Mhz (6cm), 5-10 Mhz (3cm) and 10-22 MHz (2 cm)

Table 3: Overview of the references that give a comparison between variables.

This review gives an overview of the methods used for position tracking, calibration and performance assessment in 3D ultrasound volumes formed with 2D ultrasound images. Unfortunately, an overview of these methods does not enable the comparison between different acquisition methods, as the performance depends on more variables and most authors don't give enough information about the performance affecting variables. We therefore conclude new published references should provide a more thorough overview of the variables that affect performance. This review contributes to an unified performance assessment system with an overview and categorization of the methods for position tracking, calibration and performance assessment to form a 3D ultrasound volume using 2D ultrasound images.

Conclusion

This systematic review gives an overview of the methods used for position tracking and calibration to form a 3D ultrasound volume with 2D ultrasound images. Furthermore, this review gives an overview of the performance assessment methods for 3D ultrasound volumes. The tracking methods can be categorized into: external fixture, electromagnetic tracking, optical tracking, inertial sensors and sensorless imaging. The calibration methods can be categorized into temporal or spatial calibration, with respectively three and six subcategories. As performance assessment most authors use precision or accuracy measurements, with respectively three and five calculation methods.

The increasing number of position tracking, calibration and performance assessment methods demand the comparison between methods to determine the best available 3D ultrasound acquisition method. Unfortunately, this comparison is not yet possible due to missing information on the performance-influencing variables. This review can be used to classify the methods used for position tracking, calibration and performance assessment in newly published references. Such uniform classification should simplify the comparison between different methods.

Appendix 2: Sensor initialization

Each measurement starts by touching the screen, followed by holding the probe stable for approximately 1 second. In the beginning of this first second the sensor has an initialization phase of less than 0.0001 second in which the sampling frequency is significantly higher than during the rest of the measurements. These first measurement values can be removed from the data without affecting the results. In addition, the accelerometer and gyroscope data are recorded individually with a slightly different frequency, see Figure 22. To use both sensors as if the data was recorded with the same frequency, the accelerometer data is linear interpolated to the timestamps of the gyroscope data.

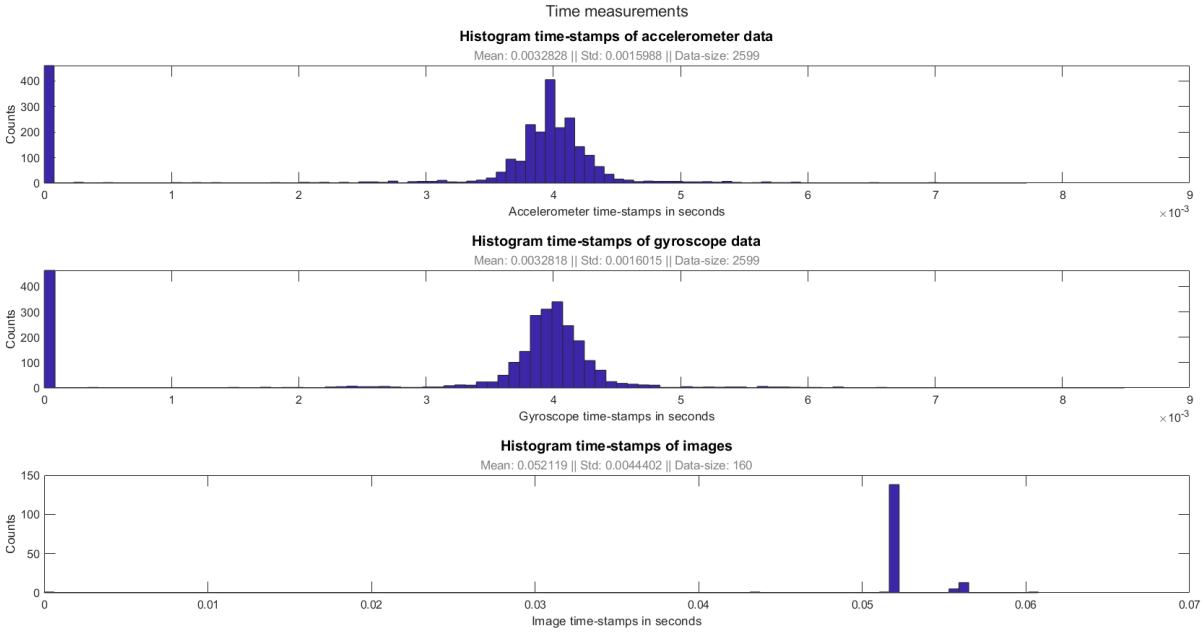

Figure 22. A histogram plot of the accelerometer and gyroscope data timestamps. Without the initialization, the accelerometer data is recorded with an average sampling of 0.003993 ± 0.00052654 per second, the data size consists of 2136 datapoints. Without the initialization, the gyroscope data is recorded with an average sampling of 0.0039921 ± 0.00053628 per second, the data size consists of 2136 datapoints. Ultrasound images are recorded with an average sampling of 0.052119 ± 0.0044402 per second, the data size consists of 160 images.

Appendix 3: Spatial calibration formulas

The spatial calibration is performed with the method described by Carbajal and Chen (Carbajal et al., 2013; Chen et al., 2009). This method uses a N-fiducial phantom, which is a horizontal 'N' as shown in Figure 23. This horizontal 'N' appears as three dots in an image plane, the image plane is represented as a red line in Figure 23. The distance between the dots in the ultrasound image and the known positions of the wires in the phantom are used to calculate the position of the middle wire crossing in world coordinates. Subsequently this position is calculated by multiplying the ultrasound coordinate with the spatial calibration matrix. The difference between these points are used in an gradient descent optimalization to calculate the best optical spatial calibration matrix. The IMU spatial calibration matrix is calculated by matrix multiplication.

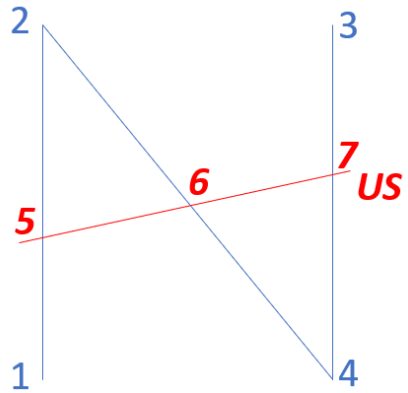

Figure 23. A systematic representation of the N-fiducial phantom. The blue lines are the lines of the phantom with known length and positions. The red line is the ultrasound image with known image coordinates.

The optical spatial calibration matrix is calculated with the following formulas. The first formula calculates the ratio between the side $|5\ 6|$ of triangle $\Delta 256$ and the side $|6\ 7|$ of triangle $\Delta 467$,

$$\mathrm{k1} = \frac{\|\mathrm{p}_7^{\mathrm{ultrasound}} - \mathrm{p}_6^{\mathrm{ultrasound}}\|}{\|\mathrm{p}_7^{\mathrm{ultrasound}} - \mathrm{p}_5^{\mathrm{ultrasound}}\|} \qquad (1)$$

, where $\mathrm{p}_\mathrm{i}^{\mathrm{ultrasound}}$ is the position of point number i in ultrasound coordinates. The second formula calculates the position of the middle wire crossing in optical coordinates:

$$\mathrm{p}_6^{\mathrm{optical}} = \mathrm{p}_3^{\mathrm{optical}} + (\mathrm{p}_1^{\mathrm{optical}} - \mathrm{p}_3^{\mathrm{optical}}) \times \mathrm{k1} \qquad (2)$$

, where $\mathrm{p}_\mathrm{i}^{\mathrm{optical}}$ is the position of point number i in optical tracking coordinates and $\mathrm{k1}$ the described ratio of formula 1. The last required formula describes an optimalization in the spatial calibration matrix to minimize the distance between the optical point and the reconstructed point:

$$\mathrm{H}_{\mathrm{ultrasound}}^{\mathrm{optical}}: \quad \min \left\| \mathrm{p}_4^{\mathrm{optical}} - \mathrm{H}_{\mathrm{ultrasound}}^{\mathrm{optical}} \times \mathrm{p}_4^{\mathrm{ultrasound}} \right\| \qquad (3)$$

, where $\mathrm{H}_{\mathrm{ultrasound}}^{\mathrm{optical}}$ is the optical spatial calibration matrix, $\mathrm{p}_4^{\mathrm{optical}}$ is point 4 in the optical coordinates and $\mathrm{p}_4^{\mathrm{ultrasound}}$ is point 4 in the ultrasound coordinates.

The IMU sensor spatial calibration matrix is calculated with the following formulas. Formula four transforms the coordinates of an ultrasound point into the coordinates of the world, using the optical tracking system as motion tracking:

$$p^{world} = H_{optical}^{world} \times H_{ultrasound}^{optical} \times p^{ultrasound} \quad (4)$$

, where p^{world} is the point in the coordinates of the world coordinate system, $H_{optical}^{world}$ the optical transformation matrix, $H_{ultrasound}^{optical}$ the optical spatial calibration and $p^{ultrasound}$ the coordinates of the point in the ultrasound image. Formula five transforms the coordinates of an ultrasound point into the coordinates of the world, using the IMU sensors as motion tracking:

$$p^{world} = H_{inertial}^{world} \times H_{ultrasound}^{inertial} \times p^{ultrasound} \quad (5)$$

, where where p^{world} is the point in the coordinates of the world coordinate system, $H_{inertial}^{world}$ the IMU sensor transformation matrix, $H_{ultrasound}^{inertial}$ the IMU sensor spatial calibration and $p^{ultrasound}$ the coordinates of the point in the ultrasound image. The fifth formula calculates the IMU sensor spatial calibration matrix with the IMU sensor transformation matrix, the optical transformation matrix and the optical spatial calibration matrix:

$$H_{ultrasound}^{inertial} = H_{optical}^{world} \times H_{ultrasound}^{optical} \times (H_{inertial}^{world})^{-1} \quad (6)$$

, where $H_{optical}^{world}$ is the optical transformation matrix, $H_{ultrasound}^{optical}$ is the optical spatial calibration, , $H_{inertial}^{world}$ the IMU sensor transformation matrix, $H_{ultrasound}^{inertial}$ the IMU sensor spatial calibration.